Molecular-level interactions between homopolypeptides and guanidinium salts and protein unfolding examined through spectroscopy and molecular modeling

Hasnain Gulamali Jaffer

A Thesis

In

The Department

Of

Chemistry and Biochemistry

Presented in Partial Fulfilment of the Requirements
for the Degree of Master of Science at
Concordia University
Montreal, Quebec, Canada

October, 2004

Canadä

Abstract

Molecular-level interactions between homopolypeptides and guanidinium salts and protein unfolding examined through spectroscopy and molecular modeling

Hasnain Gulamali Jaffer

Although many salts denature proteins (e.g. guanidine hydrochloride and guanidine thiocyanate) or stabilize them (e.g. guanidine sulfate), not much is known about salt-protein interactions at the molecular level. Using Fourier transform infrared spectroscopy (FTIR) and molecular modeling, the interaction of guanidinium salts with homopolypeptides was investigated. Evidence is presented in this thesis that these salts interact with the polypeptide side chains and not with the backbone and a model of this interaction is proposed. The temperature-dependent unfolding of horseradish peroxidase (HRPC) in the ferric and ferrous states is monitored through FTIR, two dimensional-FTIR (2D-FTIR), circular dichroism (CD) and fluorescence spectroscopies. Reduction of Fe(III) to Fe(II) in HRPC results in the appearance of high intensity aggregation bands ($1616 cm^{-1}$ and $1684 cm^{-1}$), which disappear at higher temperatures. High-resolution 2D-FTIR spectroscopy shows aggregation bands in ferric HRPC not previously observed by 1D-FTIR spectroscopy. The unfolding sequence of HRPC in both states is described and a mechanism underlying the reversible aggregation phenomena is proposed. This illustrates the usefulness of combining spectroscopy and molecular modeling in gaining molecular level information.

TABLE OF CONTENTS

CHAPTER 3: THERMAL DENATURATION OF HORSERADISH PEROXIDASE PROBED THROUGH 2D-FTIR, CD AND FLUORESCENCE SPECTROSCOPIES

LIST OF FIGURES

LIST OF TABLES

LIST OF ABBREVIATIONS AND SYMBOLS

δ, bond bending

ν, bond stretching

^{13}C-GdnDCl, deuterated and labeled with ^{13}C-guanidine hydrochloride

Asym, asymetric stretch

B3LYP, Becke 3 Lee-Yang-Parr

CD, circular dichroism spectroscopy

FTIR spectroscopy, Fourier-transform infrared spectroscopy

FW, formula weight

Gdn$^+$, guanidinium cation

Gdn$_2$D$_2$SO$_4$, deuterated guanidine sulfate

Gdn$_2$H$_2$SO$_4$, guanidine sulfate

GdnDCl, deuterated guanidine hydrochloride

GdnDSCN, deuterated guanidine thiocyanate

GdnHCl, guanidine hydrochloride

GdnHSCN, guanidine thiocyante

HF, Hartree Fock

HWHH, half-width half height

MP2, Møller Plesset

NBO, natural bond orbital

P, polypeptides

p-Arg, poly-L-arginine

p-Asn, poly-L-asparagine

p-Asp, poly-L-aspartic acid

p-Lys, poly-L-lysine

PS complex, polypeptide-associated salt

PS, polypeptide and salt mixture

S, salts

Sym, symmetric stretch

CHAPTER 1: GENERAL INTRODUCTION

Spectroscopic tools have been used to explore structural changes in biomolecules. Techniques such as Fourier-transform infrared (FTIR), 2D-IR correlation analysis, circular dichroism (CD) and fluorescence spectroscopies can provide detailed information on how certain perturbants such as temperature and/or chemical denaturants can affect biomolecular (e.g. protein) structure. Some of these techniques have also been used to study intermolecular interactions. Here, these tools have been used to examine the nature of interaction between the guanidinium salts and different homopolypeptides. Also, the use of 2D-FTIR correlation analysis, CD and fluorescence spectroscopies has been tremendously helpful in monitoring thermal denaturation of horseradish peroxidase in its ferrous and ferric forms. Below is a brief discussion of each technique used in this work.

1.1   Fourier-transform infrared (FTIR) spectroscopy

FTIR spectroscopy is a powerful technique that has traditionally been used to observe vibrations of small organic molecules. However, recently it has been reported to provide molecular level information on the structure of biomolecules.[1-6] FTIR spectroscopy of biomolecules such as proteins monitors $\nu(CO)$ and $\delta(NH)$ of the peptide bond, thereby providing information on the structure adopted by the backbone.[3] By monitoring vibrations known as amide I absorption, the secondary structure of various proteins have been characterized.[5] Generally, the amide I absorption lies between 1600 cm^{-1} and 1700 cm^{-1} and Table 1.1 summarizes the assignments of amide I absorption to secondary structures.

Table 1.1: Protein secondary structures and their characteristic amide I frequencies [7]

Secondary structures	Amide I frequencies (cm^{-1})
Aggregated strands	1610-1628
β-sheets	1625-1640
Unordered structures	1640-1648
α-helices	1648-1660
3_{10}-helices	1660-1670
β-turns	1660-1690
Antiparallel β-sheets	1675-1695

In addition, information on the tertiary structure of proteins can be obtained by studying their FTIR spectra in D_2O instead of H_2O.[5] The amide II mode lies between 1500 cm^{-1} and 1600 cm^{-1} and is mainly due to δ(NH) of the amide groups in the protein backbone.[5] The use of D_2O results in N-H/N-D exchange, which shifts the amide II absorption by ~100cm^{-1}.[3, 5] The exchange is a measure of the solvent accessibility of the amide protons. Therefore, following the intensity of the amide II band on addition of the protein to D_2O can provide information on the tertiary structure. Protons that readily exchange are exposed to the solvent, while those that are buried within the hydrophobic core or involved in strong hydrogen bonding will exchange more slowly.[3, 5]

Thus, FTIR spectroscopy is a tool that can provide molecular-level information on protein structure.

1.2   Two-dimensional correlation analysis (2D-FTIR)

The theory of two-dimensional correlation spectroscopy was developed by Noda.[8] 2D-FTIR

spectra are obtained by manipulating a group of one-dimensional dynamic spectra with

Fourier transformation.[9] The spectral components in the 2D correlation maps are plotted as a

function of the two independent spectral variables (usually in wavenumbers) and the third

axis is the spectral intensity. The 2D correlation analysis yields two plots, synchronous and

asynchronous contour plots. The peaks in the contour maps are identified as X vs. Z cm^{-1},

where X and Z represent the frequencies on the X and Z axes, respectively.

The synchronous and asynchronous maps provide details on the overall similarities and

differences respectively, of the time-dependent spectral intensity.[9, 10] Thus, the synchronous

map represents the in-phase (simultaneous) changes of the time-dependent spectral intensity.

It contains auto-peaks along the diagonal corresponding to changes in the auto-correlated

spectral intensity at a particular wavenumber. A strong auto-peak suggests large changes in

the intensity at (X, Z) upon perturbation. The synchronous map also contains cross-peaks

located off the diagonal. The cross-peaks can be either positive (solid lines) or negative

(dashed lines). Positive cross-peaks indicate that spectral intensities at the two spectral

variables (X and Z cm^{-1}) are either increasing or decreasing simultaneously due to

perturbation. On the other hand, the negative cross-peaks indicate that spectral intensities at

the two spectral variables (X and Z cm^{-1}) are increasing or decreasing in opposite

directions.[10]

The asynchronous maps represent the out-of-phase (successive) changes in spectral intensity

due to perturbation. Since asynchronous maps represent out-of-phase changes, they contain

no auto-peaks. However, they do contain positive and negative cross-peaks. According to the rules provided by Noda, a positive cross-peak at (X, Z) means that the intensity changes at X cm^{-1} precedes Z cm^{-1}, while a negative cross-peak indicates that the changes at Z cm^{-1} precede those at X cm^{-1}.[8] This rule is true if the corresponding cross peak at (X, Z) is positive in the synchronous map. If the cross peak at (X, Z) is negative in the synchronous map, then the opposite is true.

2D correlation analysis therefore provides extra information over the 1D-FTIR spectra. Two-dimensional correlation analysis has a powerful deconvolution ability and can resolve highly overlapping peaks.[9] Therefore, 2D correlation analysis offers the two-fold advantage of resolving overlapping peaks and providing a sequence of events occurring following perturbation.

1.3   Circular dichroism (CD) spectroscopy

Circular dichroism (CD) spectroscopy measures the difference in absorbance (ΔA) between left-handed (A_L) and right-handed (A_R) circularly polarized light.[7, 11] The unit of measurement is known as ellipticity (θ) and it is expressed in terms of the difference in absorbance (ΔA) or as a differential molar CD extinction coefficient ($\Delta \varepsilon$). The following equations are used to calculate ellipticity:[7, 11]

$$\theta = 33\Delta A \qquad (1)$$

$$\theta = 3300\Delta \varepsilon \qquad (2)$$

When a chromophore is in an asymmetric environment, the extent of absorption of left-handed and right-handed circularly polarized light is different. CD spectroscopy reports on this phenomenon and provides information on a chromophore's environment.

Proteins absorb in the near- and far-UV regions of CD spectra. The near-UV region lies between 250 nm and 350 nm and gives details on the environment of the aromatic residues within a protein.[7] A CD signal in this region is indicative of the presence of aromatic residues such as Phe, Tyr and Trp, and reports on their environment.[7] On the other hand, the far-UV CD absorption between 170 nm and 250 nm and arises mainly due to the peptide backbone.[7] Each secondary structure element of a protein has a specific folding pattern and a characteristic signal in the far-UV region in CD spectroscopy.[7] For example, α-helices have a strong negative peak at 222 nm, which can be monitored when the protein environment is perturbed by temperature or denaturants.[7]

1.4 Fluorescence spectroscopy

The aromatic residues such as Trp, Tyr and Phe are mainly responsible for fluorescent emission in a protein.[7, 12] In general, Trp emission dominates the fluorescence spectra since the fluorescence from Tyr and Phe is quenched by the energy transfer to Trp.[12] Trp is a better fluorescent probe relative to Tyr and Phe, when excited at a longer wavelength (295 nm). In addition, intrinsic fluorescence from Trp residues can provide information on localized structural changes since it is sensitive to the surrounding microenvironment. [7, 12]

In heme proteins, distance-dependent high-energy transfer from the fluorescent donor (Trp residues) to an acceptor (heme) occurs.[13] In folded heme proteins, Trp fluorescence is

completely quenched by the energy transfer to the heme. However, unfolding of heme proteins by temperature or denaturants results in increased fluorescence intensity. This increase in fluorescence intensity is due to the increase in Trp-heme distance. As mentioned earlier, Trp fluorescence can provide information on its surrounding environment. A red shift in Trp emission maximum signals a change from a non-polar to a polar environment.[7]

CHAPTER 2: MOLECULAR-LEVEL INTERACTIONS BETWEEN POLAR HOMOPOLYPEPTIDES AND GUANIDINIUM SALTS

2.1 Introduction

The addition of salts to protein or peptide solutions has been shown to affect solubility and stability of these solutions.[14-17] Hofmeister first demonstrated the effect of a neutral salt on the solubility of proteins.[18] Since then, many experiments have shown that the solubility of many different proteins generally follow the Hofmeister series.[19-22] The relative stability of the native and denatured states of proteins is also dependent on the nature of the salt employed. Kosmotropes (salts with salting-out properties and water-structure makers) tend to stabilize the native over the denatured state, whereas chaotropes (salts with salting-in properties and water-structure breakers) stabilize the denatured state.[22, 23] A delicate balance between two forces determines how a salt will influence the protein solubility.[24] First, the ion can directly bind to the polypeptide and affect its solubility. Second, the ion can affect the water structure around the protein based on its water structure making/breaking properties.[17, 20, 24]

A thermodynamic model of preferential hydration/exclusion proposed by Timasheff eloquently differentiates the chaotropic and kosmotropic effects of the different cations and anions found in the Hofmeister series.[16, 25-29] According to this model, small monovalent ions are bound more closely with water and therefore prefer to be associated with water rather than with polypeptides. This results in the exclusion of the ions from protein surfaces and leads to salting-out of the protein, a preferential exclusion model. On the other hand, larger ions are less tightly bound to water and prefer to be associated with proteins rather than with water, which leads to the salting-in of the proteins or preferential interaction. Timasheff

ranked the Hofmeister series of the cations and anions in order of decreasing preferential exclusion as follows: SO_4^{2-} > $MeCO_2^-$ > Cl^- > Br^- > ClO_4^- > I^- > SCN^- for the anions and NH_4^+ > Na^+ > Ba^{2+} ~ Ca^{2+} ~ Mg^{2+} > Gdn^+ for the cations.[16, 25-29] Although the effects of different salts on protein solubility and stability have been established for a long time, no detailed understanding of these phenomena is available at the molecular level. Shortle suggested that agents that promote protein denaturation act on the denatured state rather than the native state.[23] This has the effect of stabilizing the denatured state over the native state and shifting the equilibrium of native ↔ denatured states based on Le Chatelier's principle.[23] On the other hand, protein stabilizers tend to stabilize the native state over the denatured state.

In recent years, FTIR spectroscopy has been used to gain information on secondary and tertiary structures of proteins based on the $\nu(CO)$, $\nu(CN)$ and $\delta(NH)$ vibrations of the peptide bonds.[1-6] In particular, the amide I mode [80% $\nu(CO)$; 20% $\nu(CN)$] and the amide II mode [60% $\delta(NH)$; 40% $\nu(CN)$] can be used to obtain secondary and tertiary structural information, respectively. The amide I absorption lies between $1600cm^{-1}$ and $1700cm^{-1}$ while amide II absorption lies between $1500cm^{-1}$ and $1600cm^{-1}$. Secondary structures such as α-helix, β-sheet or random coil have characteristic amide I frequencies.[2-7] However, proteins are complex systems to study at the molecular level. Variations in secondary structural elements with experimental conditions complicate the spectral analysis of the amide I region. For this reason, homopolypeptides that adopt an unfolded structure within a defined pH range were selected for our studies. Poly-L-lysine (p-Lys), poly-L-aspartic acid (p-Asp), poly-L-arginine (p-Arg) and poly-L-asparagine (p-Asn) have been used as peptide models. The first three homopolypeptides have charged side-chains [3, 7, 30-33] which results in side-chain – side-

chain repulsion leading to a random coil structure.[3, 34] Poly-L-asparagine however does not have charged side-chains and has a α-helical structure around neutral pH.[7] Timasheff showed that in the presence of guanidine hydrochloride (GdnHCl) or guanidine thiocyanate (GdnHSCN) proteins were denatured, whereas guanidine sulfate ($Gdn_2H_2SO_4$) was a stabilizer.[26] To gain molecular-level information on the interaction between these salts and homopolypeptides and to determine the origin of the different effects of these salts on protein stability, we examined FTIR spectra in the amide I region.

There are experimental challenges in the use of FTIR spectroscopy to study polypeptides in the presence of guanidinium salts. First, water has a strong absorption band at 1644 cm^{-1} due to $\delta(OH)$, which overlaps with the amide I absorption of the polypeptides. To avoid this overlap, use is made of heavy water which exhibits $\delta(OD)$ at 1209 cm^{-1}, whereas the amide I' band arising mainly from $\nu(CO)$ shifts by 5 cm^{-1} or less in D_2O (amide I' where the prime indicates that the spectra were recorded in D_2O).[1-6] Second, the strong absorption of $\nu(CN)$ of guanidinium salts, centered at 1675 cm^{-1}, also overlaps with the amide I' region of the polypeptide. Deuteration of these salts red shifts $\nu(CN)$ to 1600 cm^{-1}. In addition, use of ^{13}C-labeled guanidinium salts gives rise to $\nu(^{13}CN)$ absorption at 1559 cm^{-1} in D_2O, similar to the red shift observed for $\nu(CO)$ of [13]C- labeled urea.[35-37] The third challenge lies in the spectral analysis of solutions containing high guanidinium salt concentrations since the broad $\nu(CN)$ peak overlaps with the amide I' region of the polypeptide. FTIR difference spectroscopy is a powerful technique for the detection of small spectral changes between two samples.[3, 6, 30, 31, 36-39]

2.2 Objective

The objective of the work presented in this chapter is to understand the interactions between homopolypeptides and the guanidinium salts. Specifically, the goal was to explore molecular-level interactions and to define the nature of this interaction. This may allow one to deduce why some guanidinium salts are classified as denaturants and others as stabilizers. In this work, evidence is provided that the guanidinium ion interacts with the side-chains of the homopolypeptides and that the anion plays an important role. Computational methods are employed to establish the nature of the interaction in the guanidinium-polypeptide complexes and to explain the observed blue shift in $\nu(CN)$ of guanidinium upon complexation.

2.3 Experimental section

2.3.1 Materials

Poly-L-lysine (p-Lys, M_r 52300Da), poly-L-aspartic acid (p-Asp, M_r 35600Da), poly-L-arginine (p-Arg, M_r 42400Da), poly-L-asparagine (p-Asn, M_r 10700Da), guanidine hydrochloride (GdnHCl, 99+%, FW 95.53), guanidine thiocyanate (GdnHSCN, 99+%, FW 118.2), guanidine sulfate (Gdn$_2$H$_2$SO$_4$, 99+%, FW 216.22) and D$_2$O (99.9 atom%) were purchased from Sigma, and used without any further purification. ^{13}C-labeled guanidine hydrochloride (^{13}C-GdnHCl, 99%, FW 96.53) was obtained from Isotech Inc.

2.3.2 Methods

Deuterated guanidine sulfate (Gdn$_2$D$_2$SO$_4$), guanidine-d$_5$-deuteriochloride (GdnDCl) and guanidine-d$_5$-thiocyanate (GdnDSCN) were prepared by dissolving protriated forms in D$_2$O and removing the solvent by freeze-drying on a SpeedVac (Savant, SC110). The samples

were re-dissolved in D_2O and the FTIR spectrum was recorded to confirm that H/D exchange was 100% complete. The shift in $\nu(CN)$ from 1675 cm^{-1} to 1600 cm^{-1} served as a marker for deuteration. Figure 2.1 shows deuteration of GdnHCl. ^{13}C-GdnDCl was prepared similarly to the ^{12}C salt and $\nu(^{13}CN)$ shifted to 1559 cm^{-1}. All concentrations were determined by weight.

$X = Cl^-, SCN^-, SO_4^{2-}$
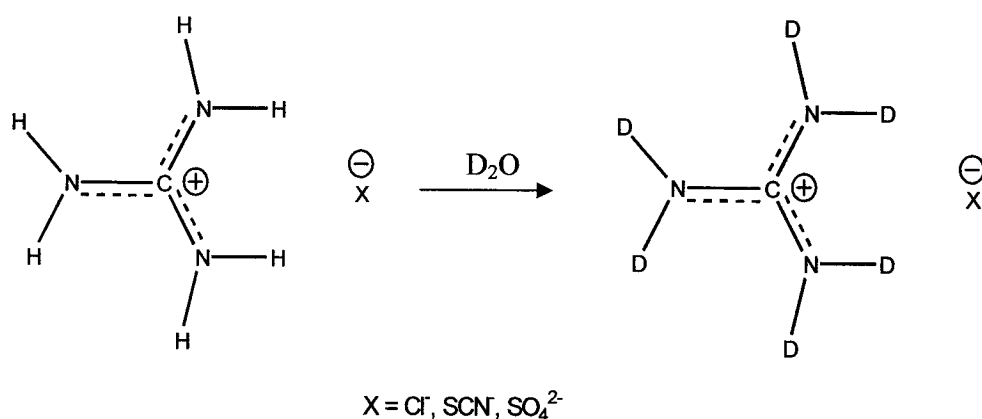
Figure 2.1: Deuteration of guanidinium cation

2.3.3 FTIR analysis

FTIR spectra were recorded using a Nicolet Magna IR 550 spectrophotometer series II equipped with a MCT/A detector purged with dry air from a Whatman Model 75-52 FTIR purge-gas generator. Data were acquired and processed using OMNIC software. Samples (7.0 μL) were placed on a CaF_2 window (13x2mm, Wildmad Inc.) of an FTIR solution cell and the cell was assembled. The cell was disassembled after each run in order to clean the windows. A small path-length (6 μm) was used due to high absorption of guanidinium at 1 M and above. All spectra represent an average of 500 scans recorded at a resolution of 2 cm^{-1} using Happ-Genzel apodization with an aperture size of 32.

FTIR difference spectra were recorded to examine the polypeptide-guanidinium interaction. The procedure consisted of first recording a spectrum of a polypeptide (spectrum P) at 25 mg/mL and a spectrum of the salt (spectrum S) at 0.5 M to 2.0 M. The polypeptide was then mixed with the salt and the spectrum PS of the mixture was recorded. The spectrum of the solvent (D_2O) was also recorded. To probe the interaction between the molecules, a series of subtractions was carried out as follows: first, the spectrum of D_2O was subtracted from each individual spectrum (spectrum P, S and PS) to remove the solvent contribution. Second, spectrum S and spectrum P were subtracted in succession from spectrum PS to remove the contribution of the free salt and of the free polypeptide from the spectrum of the PS complex. The procedure can be summarized as follows:

(1) spectrum S – spectrum D_2O = spectrum S'

(2) spectrum P – spectrum D_2O = spectrum P'

(3) spectrum PS – spectrum D_2O = spectrum PS'

(4) spectrum PS' – k_1(spectrum S') = spectrum X

(5) spectrum X – k_2(spectrum P') = difference spectrum (PS')

The δ(OD) band at 1209cm^{-1} was used as a marker to remove the contributions of the solvent in subtractions (1) to (3). Subtractions (4) and (5) were repeated until the areas under the peak and the anti-peak in the difference spectrum were approximately equal (see Figures 2.6 to 2.11). This was made possible by adjusting the subtraction factors k_1 and k_2. A normalizing factor of $1/k_2$ was found to normalize the difference spectrum to the homopolypeptide (25 mg/mL).

2.3.4 Computational analysis

Ab initio molecular orbital calculations at the Hartree-Fock (HF)[40] and at the second-order Møller-Plesset (MP2) levels of theory, [40] and hybrid density functional theory calculations at the Becke 3 Lee-Yang-Parr (B3LYP) level,[41] together with the 6-31G* basis set, were performed using the Gaussian 98 suite of programs.[42] Minimum energy structures were obtained with the Berny optimization algorithm.[43] Vibrational frequencies and thermochemical properties were then computed on the basis of the harmonic oscillator-rigid rotor model via the standard statistical mechanical expressions implemented in Gaussian 98.[44] Frequencies were scaled as described by Scott and Radom.[45] To reduce computational cost, the positively charged side chain of p-Lys is represented by methylammonium and the negatively charged side chain of p-Asp by an acetate ion. Since the interaction is electrostatic in nature, this reduced size model should account for all the important features of the salt-polypeptide interactions. The electronic structure was further characterized through Natural Bond Orbital (NBO) analysis.[46, 47] NBO describes a molecule as a Lewis-type structure by converting the molecular wavefunction into a chemically intuitive localized electron-pair bonding form.

2.4 Results

2.4.1 FTIR spectra of homopolypeptides (spectra P)

p-Lys, p-Asp and p-Arg are charged at neutral pH [3, 7, 30, 32, 33] whereas p-Asn has a neutral side chain.[7] The FTIR spectra of the three charged polypeptides show a band at ~1644 cm^{-1} which is assigned to the amide I' mode of a random coil. Electrostatic forces cause charged homopolypeptides to adopt a random coil conformation.[3, 34] In the case of p-Asn, which has a

neutral side chain, a peak at 1649 cm^{-1} is observed (Figure 2.2). This peak is assigned to the

α-helical conformation of p-Asn. The peak at 1448 cm^{-1} is assigned to the amide II' band of

the polypeptide backbone.3 This peak arises mainly from δ(ND) of the peptide bond, and

reveals that the homopolypeptides are deuterated since amide II absorption appears around

1550 cm^{-1}.3
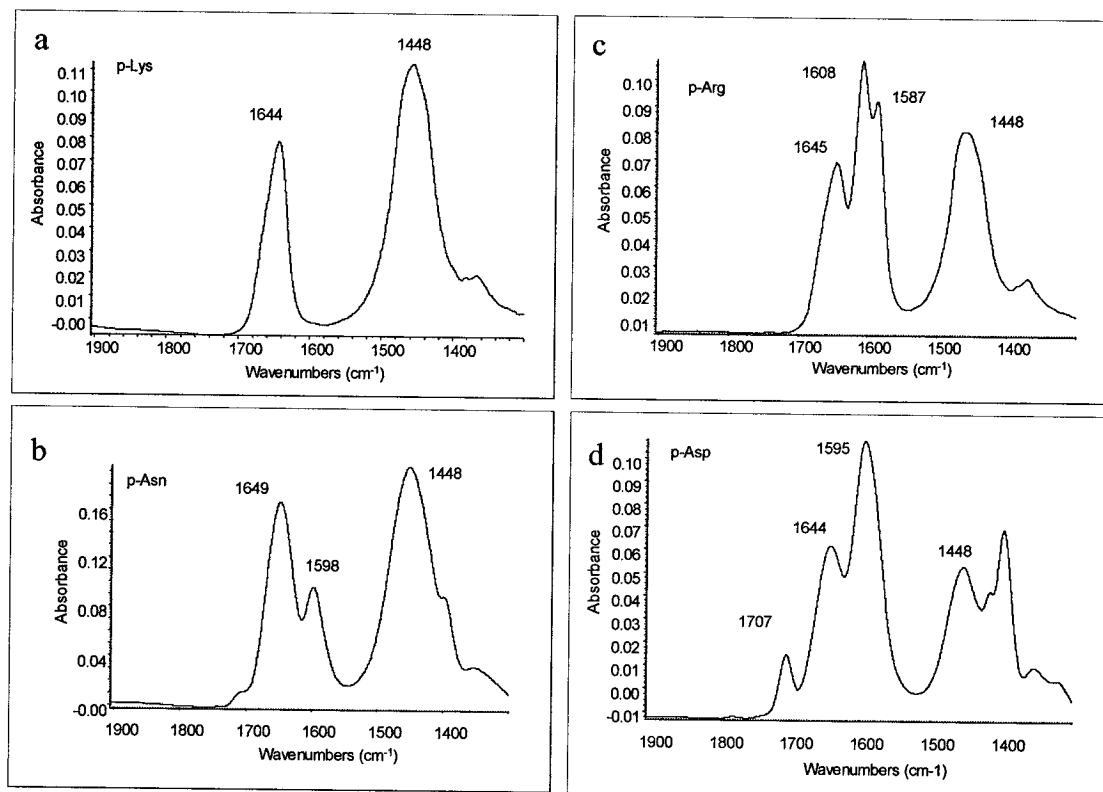
Figure 2.2: FTIR spectra of (a) p-Lys (b) p-Asn (c) p-Arg (d) p-Asp showing the amide I', amide II' and side-chain absorptions (spectra P). The FTIR spectra are an average of 500 scans acquired with a 6 μm pathlength at a resolution of 2 cm^{-1} at pH 6.2 and 25°C. Solutions were prepared by weight by dissolving the homopolypeptides in D$_2$O at a concentration of 25 mg/mL. The FTIR spectra were obtained as discussed in Section 2.3.3.

The polypeptide side chains also absorb in amide I' region. In the case of p-Asp, the

carboxylate asymmetric stretch $v(COO^-)$ and the carbonyl $v(COOD)$ are found at 1595 cm^{-1}

and 1707 cm^{-1}, respectively. In p-Arg, $v(CN_3D_6^+, sym)$ and $v(CN_3D_6^+, asym)$ absorb at 1587

cm^{-1} and 1608 cm^{-1}, respectively and in p-Asn, $v(CO)$ absorbs at 1598 cm^{-1}. In p-Lys $v(ND_3^+)$ absorbs at 1625 cm^{-1} but the very weak band is not observed.[32] Table 2.1 summarizes the side-chain absorption of all four homopolypeptides. These assignments are based on the results of a study of the free amino acid study in H_2O by Venyaminov and Kalnin.[32]

Table 2.1: Side-chain absorptions of different homopolypeptides within the amide I' region[a]

Homopolypeptide	Wavenumber (cm^{-1})	Assignment
p-Lys	1629	$v(ND_3^+)$
p-Arg	1608	$v(CN_3D_6^+)$, asym
	1587	$v(CN_3D_6^+)$, sym
p-Asp	1707	$v(COOD)$
	1595	$v(COO^-)$
p-Asn	1598	$v(CO)$

[a]These wavenumbers are deduced from studies on free amino acid in H_2O by Venyaminov and Kalnin.[32]

2.4.2 FTIR spectra of GdnDCl, GdnDSCN and Gdn$_2$D$_2$SO$_4$ (spectra S)

Figure 2.3 shows the partial FTIR spectra of 0.5 M to 2.0 M GdnDCl in D_2O. The $v(CN)$ absorption intensities at 1600 cm^{-1} (asymmetric) increases linearly with GdnDCl concentration, while the peak at 1209 cm^{-1} due to $\delta(OD)$ of the D_2O solvent decreases slightly at higher salts concentrations. Deuteration of GdnHCl results in a red shift of $v(CN)$ from 1675 cm^{-1} to 1600 cm^{-1}, which further red-shifts to 1559 cm^{-1} in ^{13}C-GdnDCl (see Appendix A). GdnDSCN and Gdn$_2$D$_2$SO$_4$ also exhibit $v(CN)$ absorption at 1600 cm^{-1}. The anions absorb as follows: $v(SCN)$ at 2064 cm^{-1} (Figure 2.4) and $v(SO_4)$ at 1104 cm^{-1} (see Appendix B).
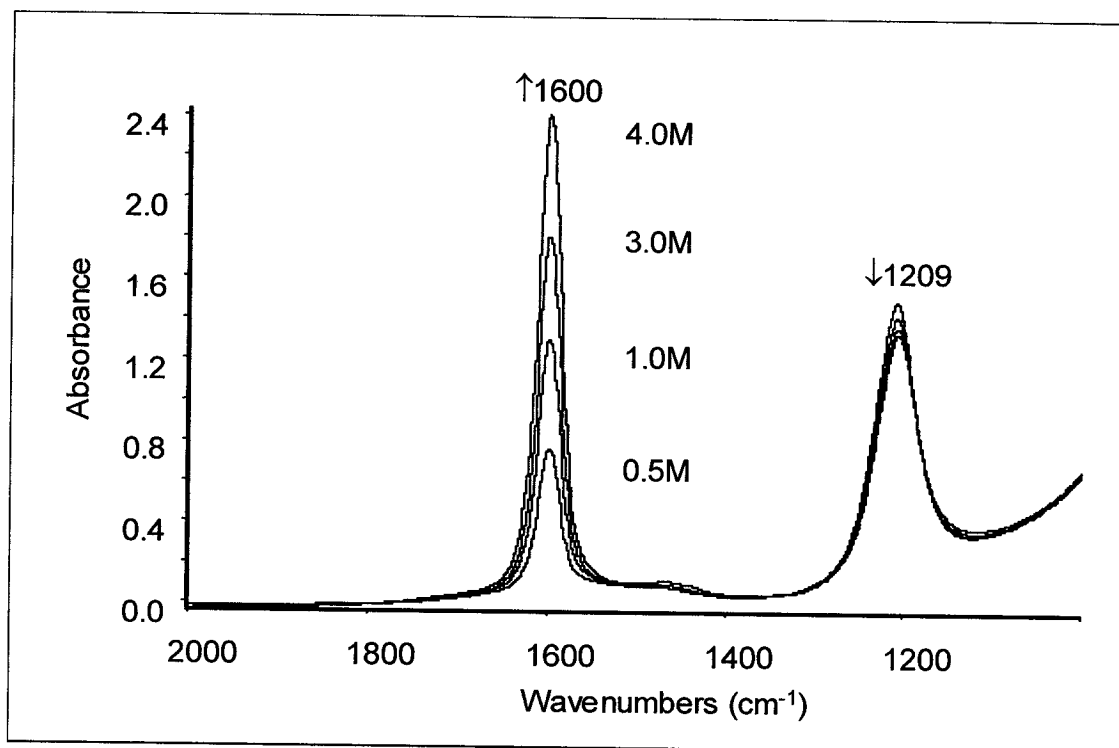
Figure 2.3: FTIR spectra of GdnDCl showing v(CN) with increasing concentration (spectra S). The peak at 1600 cm⁻¹ and 1209 cm⁻¹ are assigned to v(CN) of GdnDCl and δ(OD) of D_2O, respectively. The FTIR spectra are an average of 500 scans acquired with a 6 μm pathlength at a resolution of 2 cm⁻¹ at pH 6.2 and 25°C. Solutions were prepared by weight by dissolving the salt in D_2O and the FTIR spectra were obtained as described in Section 2.3.3. The up arrows (↑) indicate an increase in intensity while the down arrows (↓) a decrease in intensity with increasing concentration of the salt.
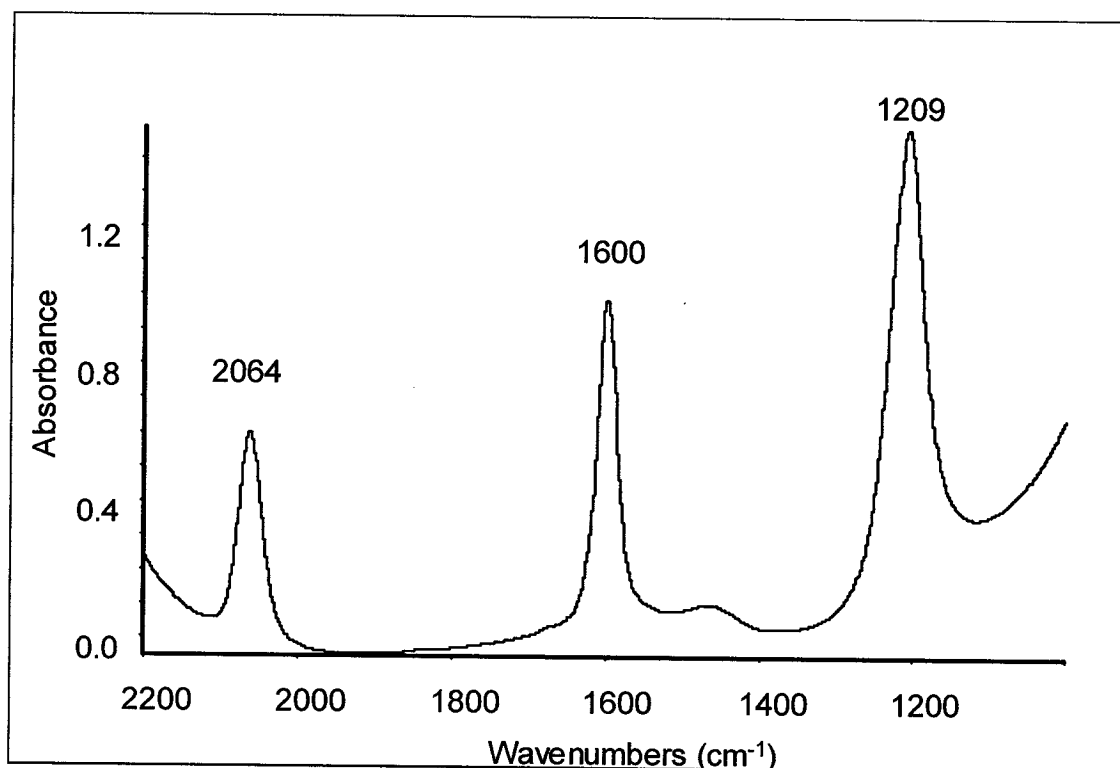
Figure 2.4: FTIR spectrum of 1 M GdnDSCN. The peaks at 1600 cm^{-1} and 1209 cm^{-1} are assigned to v(CN) of GdnDSCN and δ(OD) of D$_2$O, respectively. A distinct peak at 2064 cm^{-1} is assigned to v(SCN). The FTIR spectrum is an average of 500 scans acquired with a 6 μm pathlength at a resolution of 2 cm^{-1} at pH 6.2 and 25°C. FTIR spectra were obtained as described in Section 2.3.3.

2.4.3 FTIR spectra of polypeptide and salt mixtures (spectra PS)

Figure 2.5 shows the spectra of solutions of p-Lys and GdnDCl. The spectra are dominated by the asymmetric 1600 cm^{-1} v(CN) absorption of guanidinium, and the contribution of the polypeptide backbone at 1644 cm^{-1} is very small. The other homopolypeptide/salt solutions exhibit similar spectra to those shown in Figure 2.5 for p-Lys/GdnDCl. Since the spectra are dominated by free Gdn$^+$ absorption, difference spectra were generated to look for small changes upon binding of Gdn$^+$ to the homopolypeptides.

↑1600

2.0 M

1.5 M

↓1209

1.0 M

0.5 M

1644   1448

2.0
1.6
1.2
0.8
0.4
0.0

Absorbance

2000   1800   1600   1400   1200

Wavenumbers (cm⁻¹)
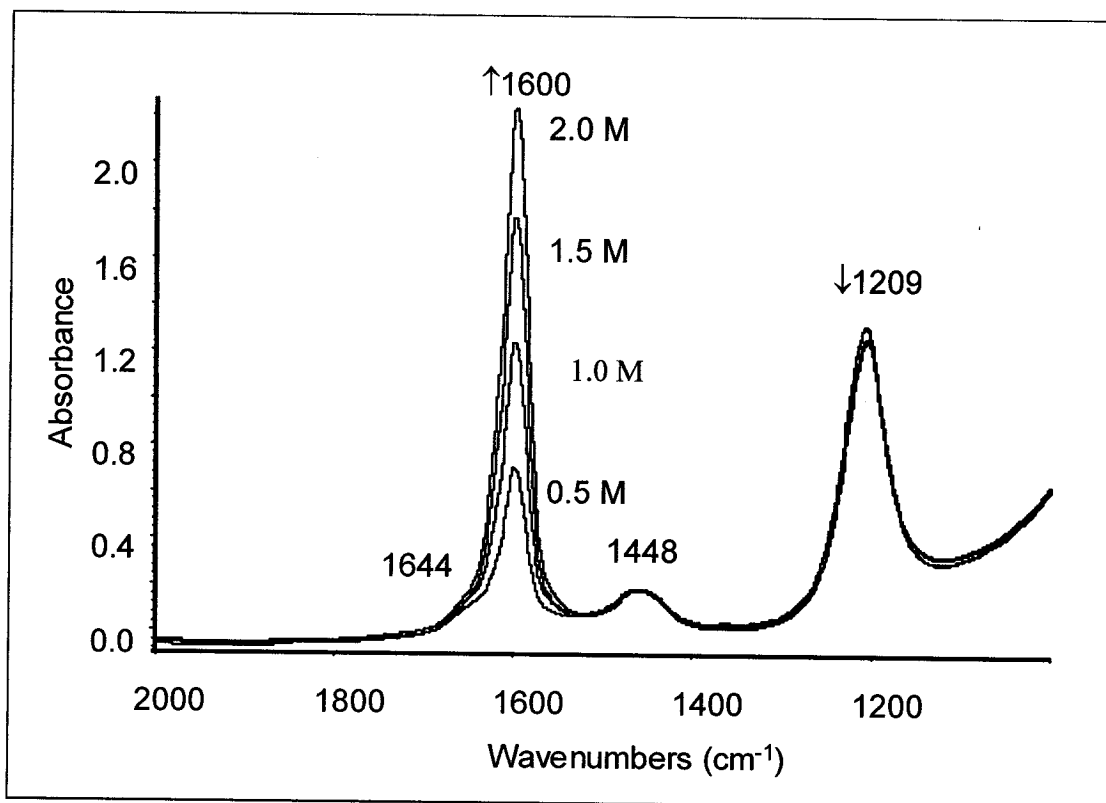
Figure 2.5: FTIR spectra of a mixture of GdnDCl and p-Lys showing v(CN) with increasing concentrations of the salt (spectra PS). The peaks at 1600 cm⁻¹ and 1209 cm⁻¹ are assigned to v(CN) of GdnDCl and δ(OD) of D₂O, respectively. The shoulder at ~1644 cm⁻¹ and a slightly higher peak at 1448 cm⁻¹ are due to amide I'and amide II' bands of the p-Lys, respectively. The FTIR spectra are an average of 500 scans acquired with a 6 μm pathlength at a resolution of 2 cm⁻¹ at pH 6.2 and 25°C. The salt solution at each concentration was mixed with 25 mg/mL of p-Lys and the FTIR spectra were obtained as described in Section 2.3.3. The up arrows (↑) indicate an increase in intensity while the down arrows (↓) a decrease in intensity with increasing concentration of the salt.

2.4.4 Interaction between the homopolypeptides and the salts

Figure 2.6 shows difference spectra PS' (section 2.2.3) in presence of p-Lys. A peak at 1622 cm⁻¹ and an anti-peak at ~1595 cm⁻¹ dominate the spectra. Adjusting the subtraction factors (k₁ and k₂) such that the areas under the peak and the anti-peak are similar at each concentration gives rise to a straight baseline from ~1640 cm⁻¹ to 1850 cm⁻¹. If there were no interaction between GdnDCl and p-Lys, subtractions (1) to (5) would cancel each other and a

straight line would result. Obviously, the two solutes interact, giving rise to a difference peak at 1622 cm^{-1} and another anti-peak at 1595 cm^{-1} which is close to v(CN) of free GdnDCl (Figure 2.6). Thus, the anti-peak is assigned to free GdnDCl while the peak at 1622 cm^{-1} is assigned to polypeptide-associated GdnDCl (PS complex). Since the intensity of the 1622 cm^{-1} peak is very weak, it is unclear whether it is due to symmetric or antisymmetric stretch.
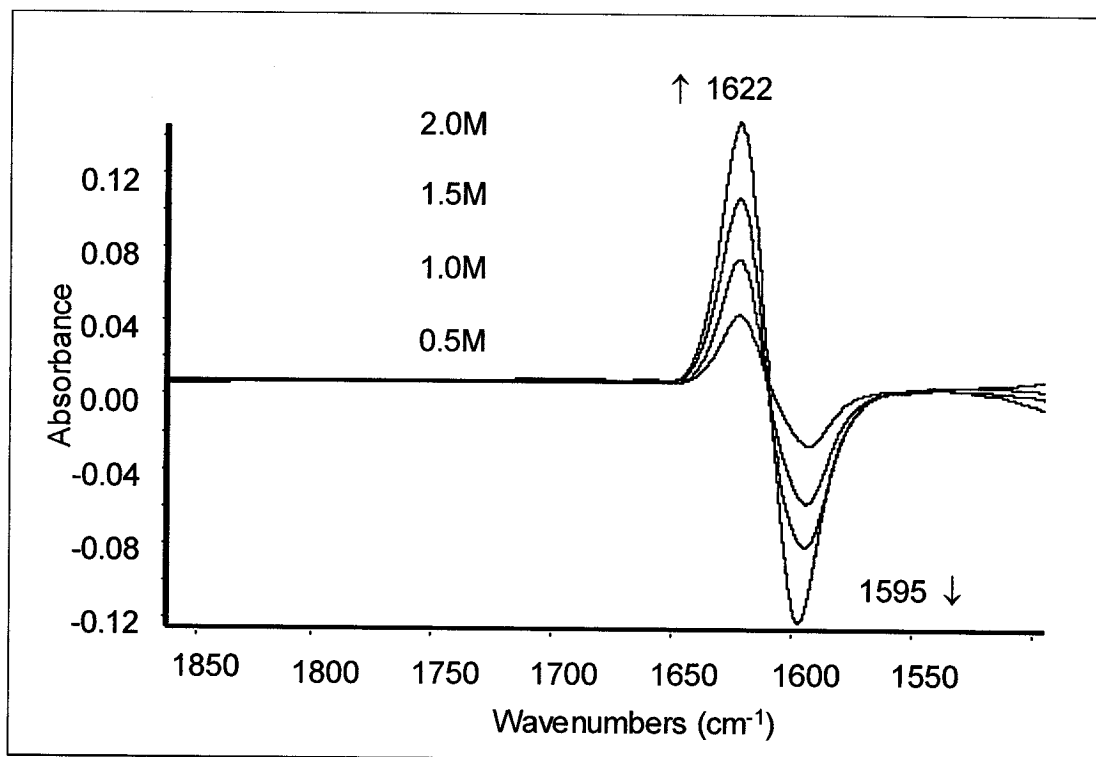
Figure 2.6: FTIR difference spectra of GdnDCl in the presence of 25 mg/mL p-Lys at pH 6.2 and 25°C. A linear increase in the PS absorbance is observed with increasing concentration of GdnDCl from 0.5 M to 2.0 M. The peak at 1622 cm^{-1} is assigned to p-Lys-associated GdnDCl, which is referred to as the PS complex. The anti-peak at 1595 cm^{-1} is assigned to the free salt. The FTIR difference spectra were obtained as described in Section 2.3.3. The up arrows (↑) indicate an increase in intensity while the down arrows (↓) a decrease in intensity with increasing concentration of the salt.

2.4.5 Changes in v(CN) of the salt

[13]C labeling of the guanidinium ion results in a red shift of v(CN) from 1600 to 1559 cm^{-1} in D_2O (see Appendix A and Figure 2.3). If the difference peaks observed in Figure 2.6 are due

19

to the v(CN) absorption of GdnDCl, then the peak at 1622 cm^{-1} and the anti-peak at ~1595

cm^{-1} should also red-shift upon ^{13}C labeling. Indeed, Figure 2.7 shows that these peaks are

red-shifted to 1588 cm^{-1} (PS' complex) and 1559 cm^{-1}, respectively. A weak difference peak

is also observed at ~1654 cm^{-1}, which may be due to some α-helical formation in the

polypeptide backbone upon association with the salt. However, the intensity of this band

relative to the intensity of the band assigned to v(^{13}CN) of the PS' complex is negligible,

suggesting that only a small fraction of the polypeptide adopts a α-helical conformation. The

weak shoulder at ~1627 cm^{-1} is due to side-chain shifts and is further discussed in Section

2.3.9.
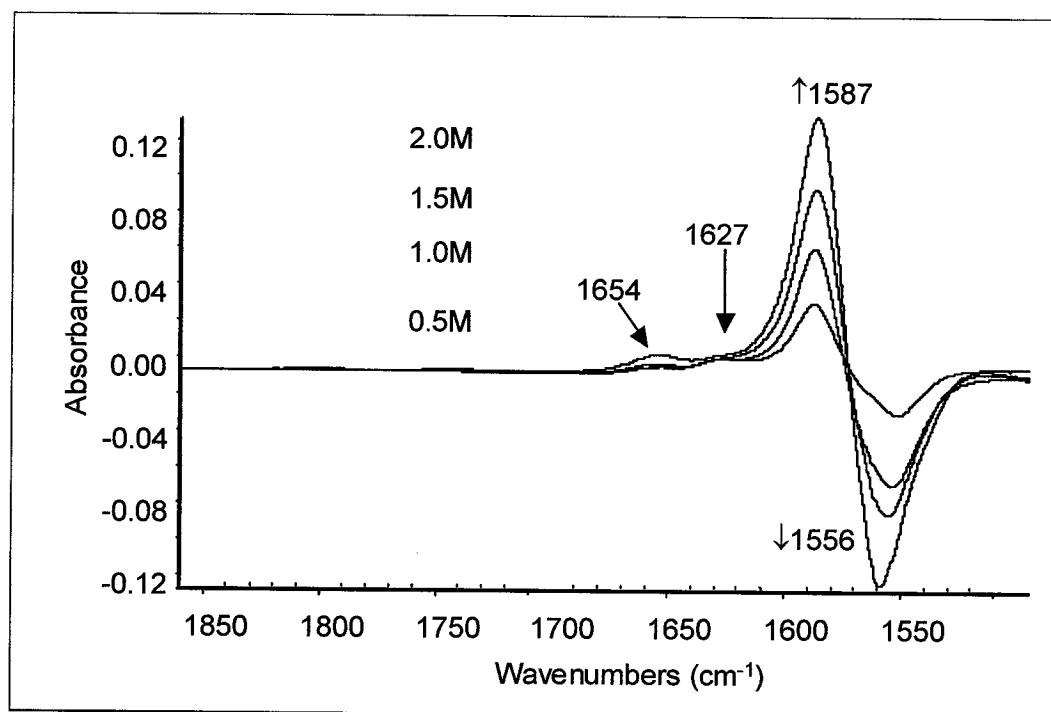
Figure 2.7: FTIR difference spectra of ^{13}C-GdnDCl in the presence of 25 mg/mL p-Lys at pH 6.2 and 25°C. A linear increase in the PS' complex with increasing concentrations of ^{13}C-GdnDCl from 0.5 M to 2.0 M. The peak at 1587 cm^{-1} is assigned to the p-Lys-associated ^{13}C-GdnDCl referred to as PS' complex. The anti-peak at 1556 cm^{-1} corresponds to the free salt. The peak at 1627 cm^{-1} is due to the polypeptide side-chain shifts whereas the peak at 1654 cm^{-1} is due to α-helical conformation of the polypeptide backbone. The FTIR difference spectra were obtained as described in Section 2.3.3. The up arrows (↑) indicate an increase in intensity while the down arrows (↓) a decrease in intensity with increasing concentration of the salt.

2.4.6 Difference spectra of GdnDCl, ^{13}C-GdnDCl, GdnDSCN and Gdn$_2$D$_2$SO$_4$

Figures 2.8 to 2.11 show difference spectra for the four homopolypeptides in 1 M GdnDCl, ^{13}C-GdnDCl, GdnDSCN and 0.5 M Gdn$_2$D$_2$SO$_4$. Although difference spectra at a single concentration of the salt are shown here, band intensities are guanidinium concentration-dependent as seen in Figure 2.6. In all cases shown in Figures 2.8 to 2.11, a blue-shift in ν(CN) of the guanidinium is observed upon association with the homopolypeptides. For example, ν(CN) shifts from ~1600 to ~1622 cm^{-1} upon association with the polypeptide in Figure 2.8. In the p-Asp/GdnDCl difference spectrum, a small anti-peak at 1710 cm^{-1} and a peak at 1692 cm^{-1} are observed, suggesting that ν(COOD) of p-Asp red-shifts in the presence of GdnDCl (Figure 2.8d). The ν(^{13}CN) peak and the anti-peak are red-shifted in Figure 2.9 due to the mass effect in ^{13}C-GdnDCl. The low-intensity peak at ~1654 cm^{-1} in the p-Lys/^{13}C-GdnDCl difference spectra (Figure 2.9a) is assigned to formation of an α-helical structure in the p-Lys upon association with the salt. The shoulder at ~1627 cm^{-1} (Figure 2.9) arises from side-chain shifts as discussed below in Section 2.4.9. Figures 2.10 and 2.11 reveal that the difference spectra of the polypeptides in the presence of GdnDSCN and Gdn$_2$D$_2$SO$_4$ are similar to those for GdnDCl in that ν(CN) is blue-shifted. Low intensity peaks at ~1654 cm^{-1}, 1670 cm^{-1} to 1678 cm^{-1} are assigned to small conformational changes in the polypeptide as mentioned above.
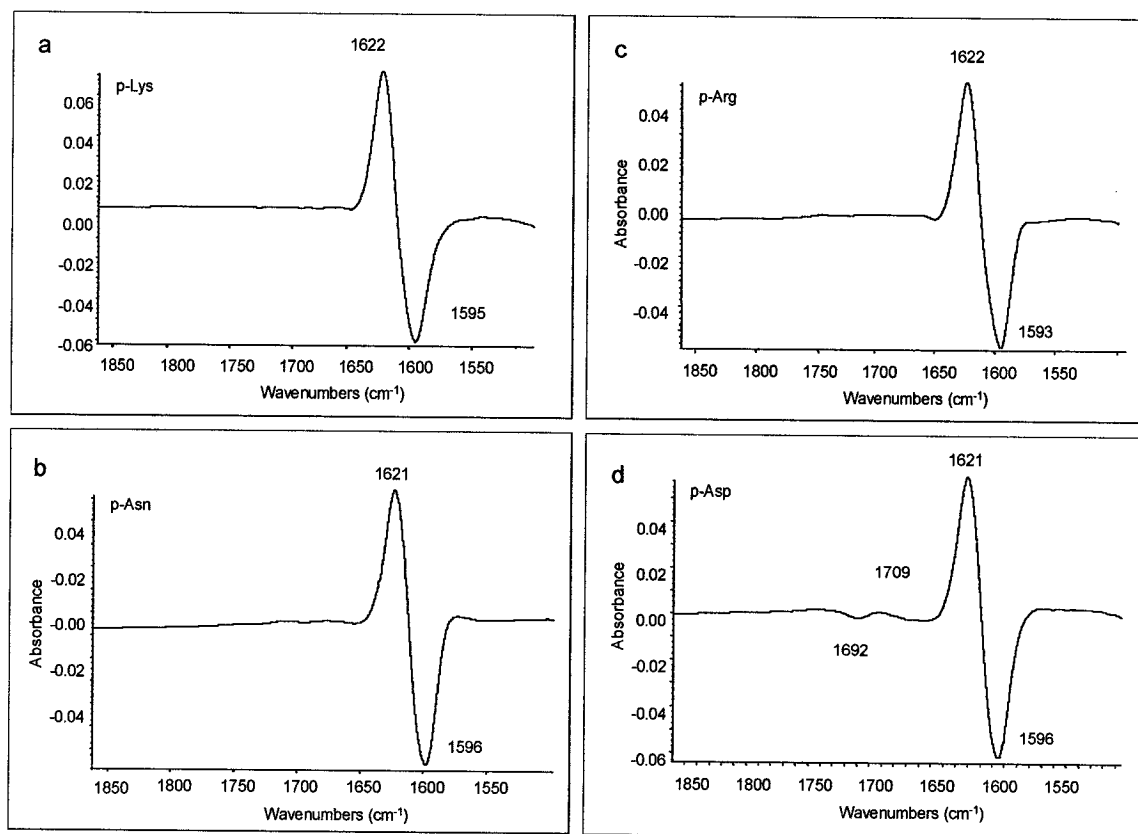
Figure 2.8: FTIR difference spectra of 1 M GdnDCl in the presence of (a) p-Lys (b) p-Asn (c) p-Arg (d) p-Asp at pH 6.2 and 25°C. Similar blue-shifts in $v(CN)$ of guanidinium are observed in presence of all homopolypeptides at 25 mg/mL. The peak at ~1622 cm^{-1} is assigned to the polypeptide-associated GdnDCl referred to as the PS complex. The anti-peak corresponds to free salt. The small anti-peak at 1709 cm^{-1} and a peak at 1692 cm^{-1} suggest that $v(COOD)$ of p-Asp red shifts in the presence of GdnDCl. The FTIR difference spectra were obtained as described in Section 2.3.3.
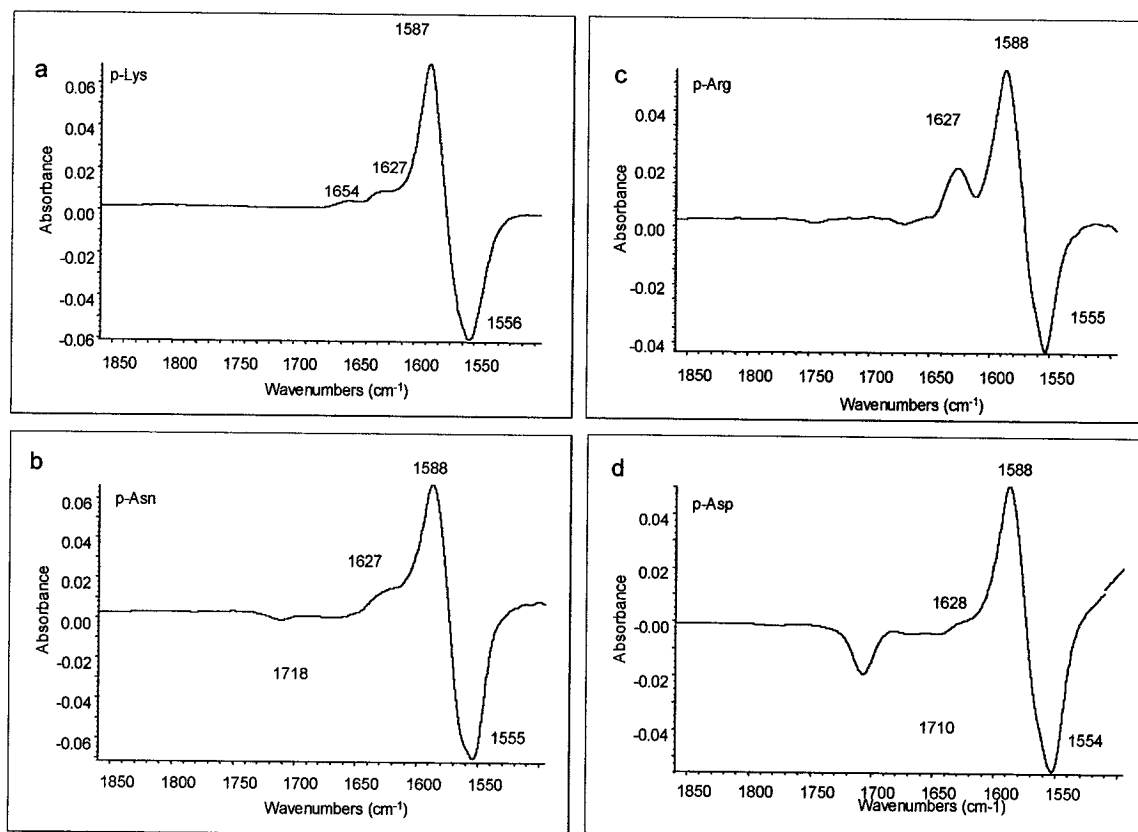
Figure 2.9: FTIR difference spectra of 1 M ^{13}C-GdnDCl in the presence of (a) p-Lys, (b) p-Asn, (c) p-Arg, and (d) p-Asp at pH 6.2 and 25°C. Similar blue shifts in $v(^{13}CN)$ of guanidinium are observed in the presence of all homopolypeptides at 25 mg/mL. The peak at ~1588 cm^{-1} is assigned to the polypeptide-associated ^{13}C-GdnDCl referred to as the PS' complex. The anti-peak corresponds to the free salt. The shoulder at ~1627 cm^{-1} is assigned to side-chain upon association with the salt. The weak absorbance at ~1655 cm^{-1} is assigned to polypeptide conformational changes, and the strong negative peaks at 1710 cm^{-1} and 1718 cm^{-1} are assigned to $v(COOD)$ and $v(COND_2)$ of p-Asp and p-Asn side chain shifts, respectively described in Section 2.4.6. The FTIR difference spectra were obtained as described in the Section 2.3.3.
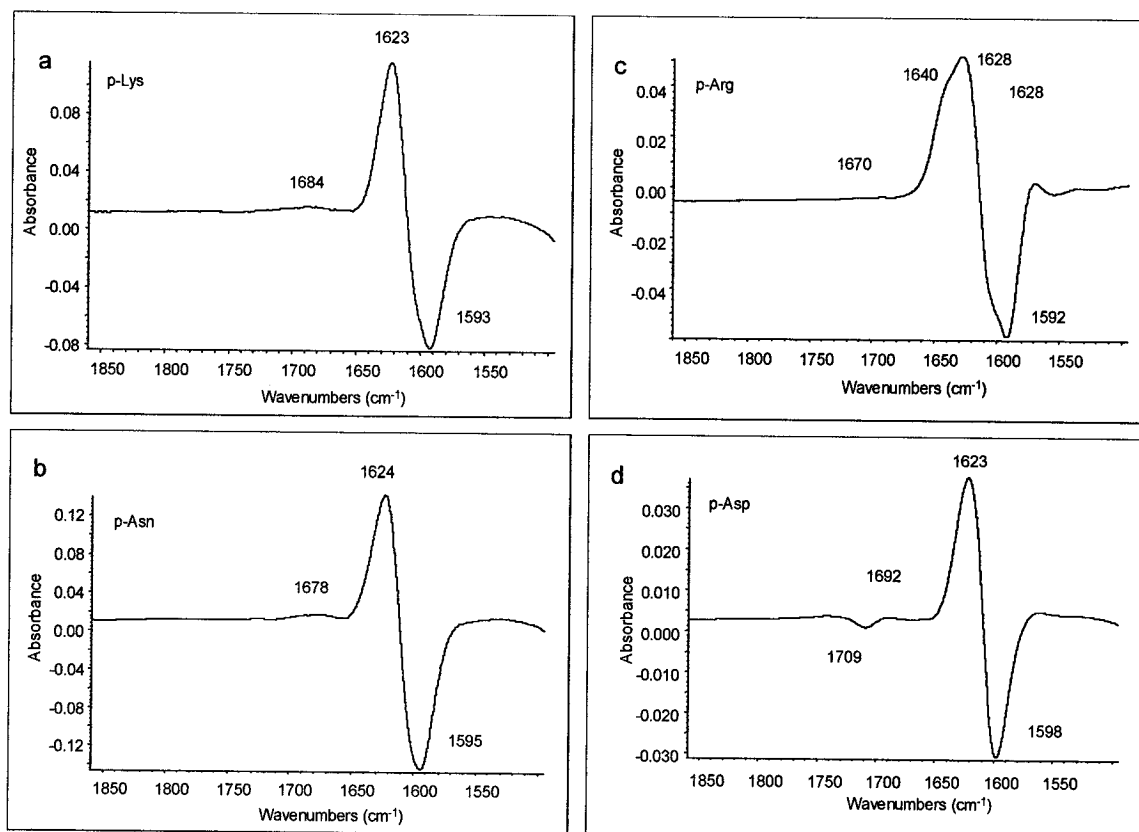
Figure 2.10: FTIR difference spectra of 1 M GdnDSCN in presence of (a) p-Lys, (b) p-Asn, (c) p-Arg, and (d) p-Asp at pH 6.2 and 25°C. Similar blue shifts in ν(CN) of guanidinium are observed in presence of all homopolypeptides at 25 mg/mL. The peak at ~1623 cm^{-1} is assigned to the polypeptide-associated GdnDSCN referred to as the PS complex. The anti-peaks at 1593 cm^{-1} – 1598 cm^{-1} correspond to the free salt. Slight perturbation in most polypeptides occur at ~1670 cm^{-1} - 1684 cm^{-1} due to small polypeptide conformational changes. The small anti-peak at 1709 cm^{-1} and a peak at 1692 cm^{-1} suggest that ν(COOD) of p-Asp red shifts in the presence of GdnDSCN. The FTIR difference spectra were obtained as described in Section 2.3.3.
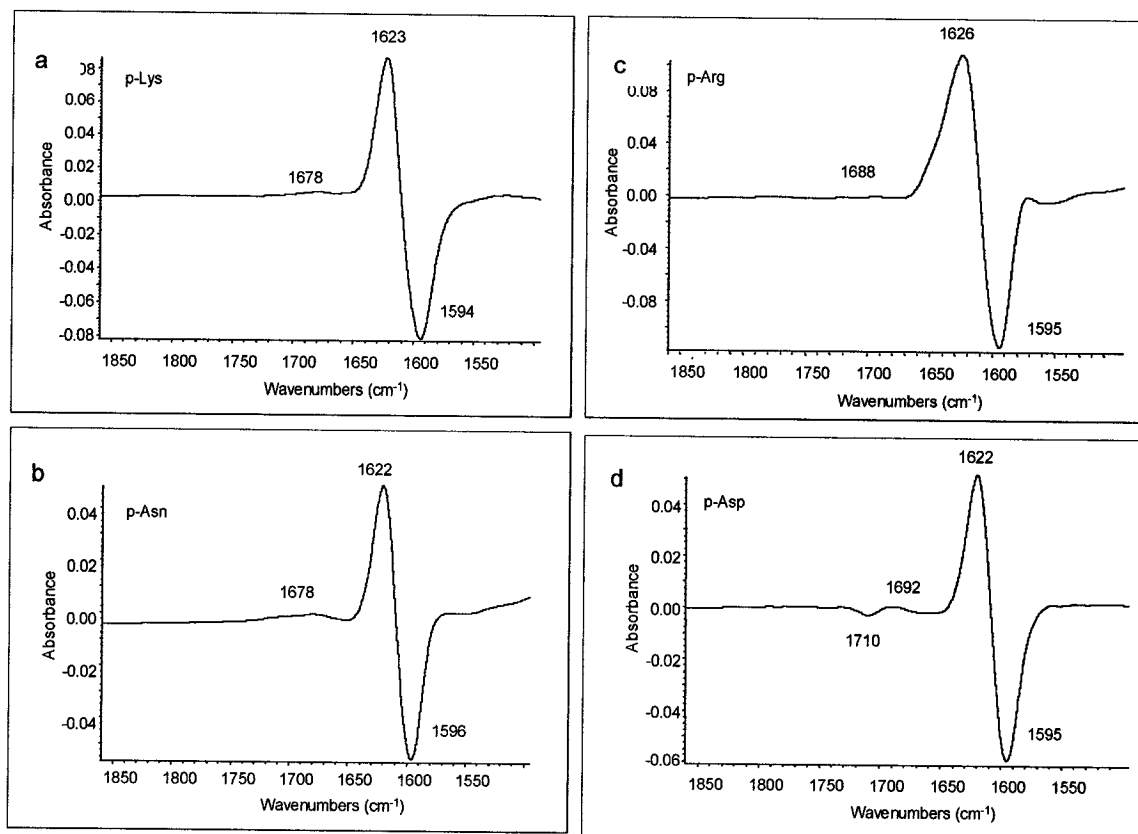
Figure 2.11: FTIR difference spectra of 0.5 M $Gdn_2D_2SO_4$ in presence of (a) p-Lys, (b) p-Asn, (c) p-Arg, and (d) p-Asp at pH 6.2 and 25°C. Similar blue shift in $\nu(CN)$ of guanidinium is observed in presence of all homopolypeptides at 25 mg/mL. The peak at ~1623 cm^{-1} is assigned to polypeptide-associated $Gdn_2D_2SO_4$ referred to as the PS complex. The anti-peak at 1594 cm^{-1} – 1596 cm^{-1} corresponds to free salt. Slight perturbation in most polypeptides occur at ~1678 cm^{-1} – 1688 cm^{-1} probably due to small polypeptide conformational changes. The small anti-peak at 1710 cm^{-1} and a peak at 1692 cm^{-1} suggest that $\nu(COOD)$ of p-Asp red shifts in the presence of $Gdn_2D_2SO_4$. The FTIR difference spectra were obtained as described in Section 2.3.3.

25

The ^{13}C-GdnDCl/p-Lys difference spectra in Figure 2.7 reveal negligible amide I' absorption

of the polypeptide. Hence, guanidinium salts are unlikely hydrogen-bonded to the

polypeptide backbone. Careful examination of Figures 2.8 to 2.11 shows small difference

bands at ~1670 cm^{-1} - 1688 cm^{-1} depending on the salt and polypeptide. However, their

intensities are much weaker compared to the peak at 1622 cm^{-1} (or 1587 cm^{-1} for ^{13}C-

GdnDCl). Therefore, it is speculated that the guanidinium salts interact with the polypeptide

side chains and not the backbone.

2.4.7 Model of interaction between the salts and the homopolypeptides

Figure 2.12 shows a proposed model of interaction between the salts and homopolypeptides.

In the case of p-Lys and p-Arg, which have positively charged side chains, the anion X$^-$

(where X$^-$ = Cl$^-$, SCN$^-$ or SO$_4^{2-}$) acts as a bridge between Gdn$^+$ and the side chain. However,

in p-Asp, Gdn$^+$ interacts directly with the negatively charged side chain. If these interaction

models were correct, ν(SCN$^-$) would be sensitive to the nature of the side-chain, and the side-

chain absorption of the polypeptide would shift upon association with the salts.

Guanidinium salt with p-Lys

26

Guanidinium salt with p-Asp

b)
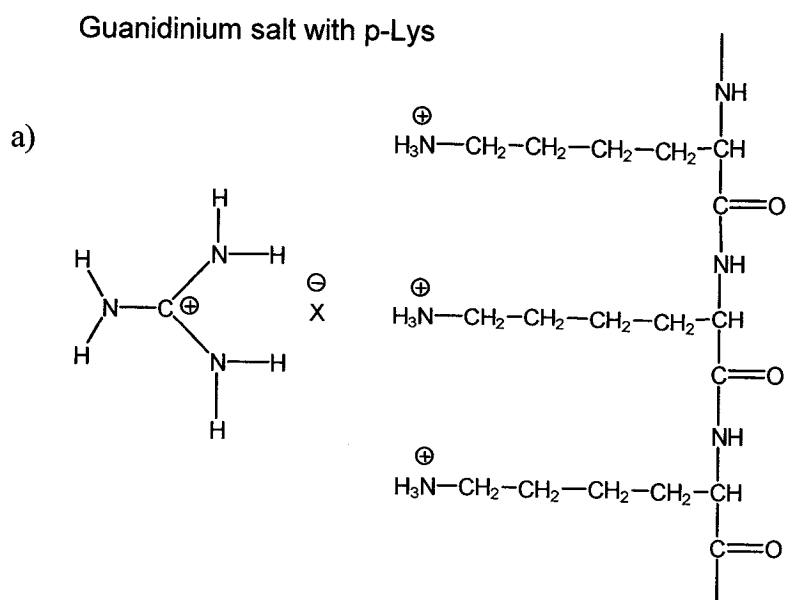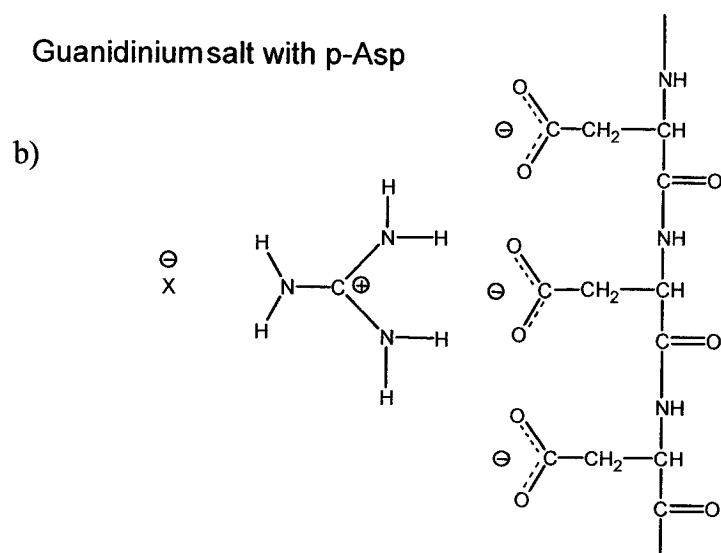
Figure 2.12: Model of interaction of GdnX with p-Lys and p-Asp. Depending on the charge on the polypeptide side chain, the anion behaves differently. In the case of positively charged side chains, the anion acts as a bridge between the side chain and the guanidinium cation. The guanidinium cation directly interacts with negatively charged side chains. The anion X⁻ is Cl⁻, SCN⁻ or SO_4^{2-}.

2.4.8 The role of the anion

The peak at 2064 cm⁻¹ in the FTIR spectrum of 1 M GdnDSCN in D_2O (Figure 2.4) is assigned to free ν(SCN⁻). Figure 2.13 shows the difference spectra of GdnDSCN in the presence of the homopolypeptides. A difference anti-peak is observed at ~2064 cm⁻¹ in each spectrum and a difference peak at ~2045 cm⁻¹ or 2078 cm⁻¹, which is assigned to the polypeptide associated anion. Thus, the association with the positively charged residues (p-Lys and p-Arg), red shifts ν(SCN⁻) from 2064 cm⁻¹ to ~2044 cm⁻¹, whereas in the presence of the negatively charged p-Asp, a blue shift from 2060 cm⁻¹ to 2078 cm⁻¹ occurs. The different behavior of the anion validates our proposed model. In the presence of p-Asn (neutral residues), ν(SCN⁻) undergoes a red shift similar to that observed in the presence of p-Lys and p-Arg, suggesting that the anion is acting as a bridge between Gdn⁺ and the p-Asn side

27

chains. Since $\nu(SO_4^{2-})$ of $Gdn_2D_2SO_4$ overlaps with $\delta(OD)$, changes in $\nu(SO_4^{2-})$ of

$Gdn_2D_2SO_4$ could not be successfully monitored in D_2O.
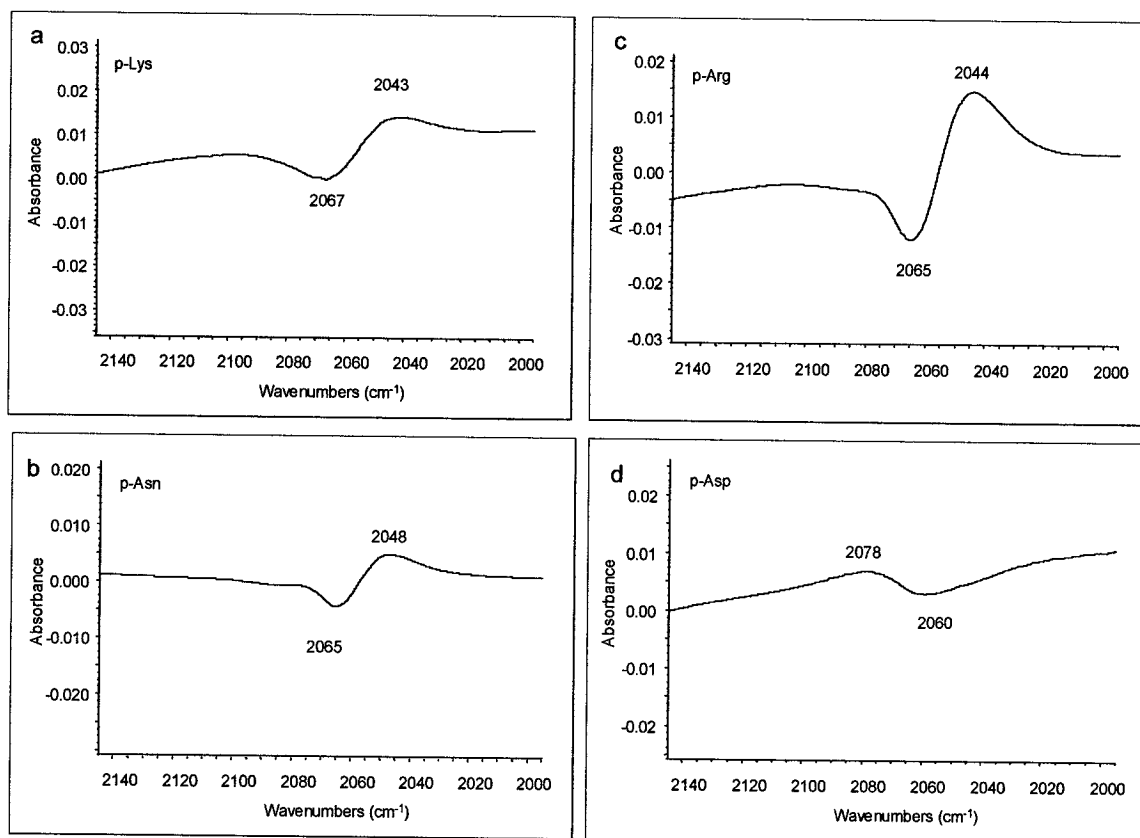
Figure 2.13: FTIR difference spectra of 2.0 M GdnDSCN in the presence of (a) p-Lys, (b) p-Asn, (c) p-Arg, and (d) p-Asp at pH 6.2 and 25°C. The peaks at ~2043 cm^{-1} in p-Lys, p-Arg and p-Asn and at 2078 cm^{-1} in p-Asp are assigned to $\nu(SCN^-)$ of polypeptide-associated GdnDSCN while the anti-peaks are assigned to free GdnDSCN. A red-shift in $\nu(SCN^-)$ is observed in the presence of positively charged and neutral side chains, whereas a blue-shift is observed in the presence of p-Asp. The FTIR difference spectra were obtained as described in Section 2.3.3.

2.4.9 Side-chain bands

Figure 2.9 shows a weak shoulder appearing at ~1627 cm^{-1} in presence of p-Asn, p-Asp and

p-Lys difference spectra whereas a distinct peak at ~1627 cm^{-1} is present in the p-Arg

spectrum. This absorption is attributed to blue shifted bands of the side-chain upon

association with the ^{13}C-GdnDCl. These peaks are only apparent in Figure 2.9 since the

polypeptide side-chain absorption is masked by $v(CN)$ of the PS complex in Figures 2.6, 2.8, 2.10 and 2.11. A strong peak is observed in the p-Arg/GdnDCl difference spectrum due to the strong absorption of the guanidinium asymmetric stretch $v(CN_3D_6^+)$ (see Figure 2.2a). However, the ~1627 cm^{-1} difference peak may also be due to $v(CN)$ of trace unlabeled GdnDCl present in 1 M ^{13}C-GdnDCl.

2.4.10 Computational analysis of Gdn$^+$, GdnHCl and PS complex

2.4.10.1 Free GdnHCl

Two configurations of free GdnHCl were found that vary in the position of the chloride ion (Figure 2.14). In configuration A the chloride ion lies above the plane of the guanidinium ion, while in configuration B it lies in the plane of the guanidinium ion. The relative Gibbs free energies shown in Table 2.2 indicate that configuration B is the more stable species due to the weak hydrogen bonds between the chloride ion and the amine groups, which are represented by dashed lines (Table 2.2).

(a)

(b)
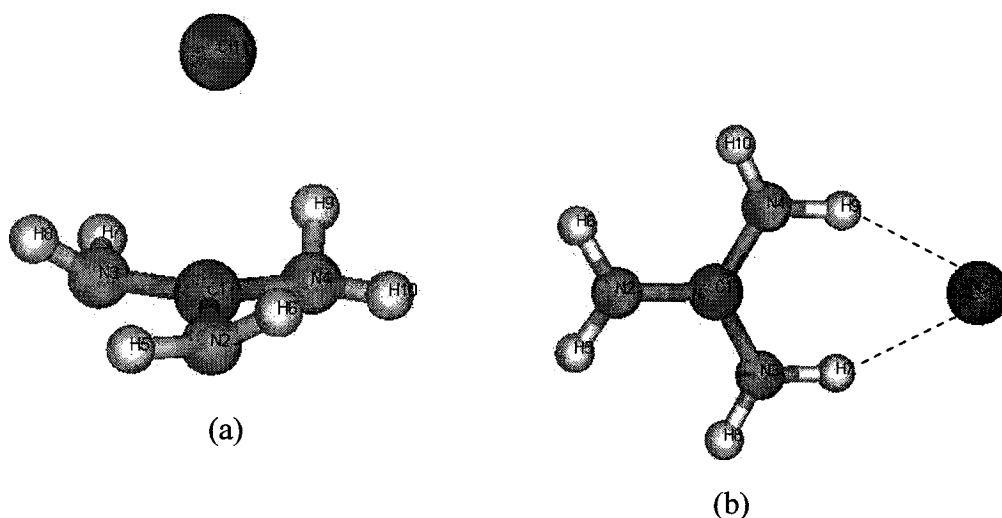
Figures 2.14: Two configurations of free GdnHCl with the chloride anion above the plane (a) and in the plane (b) of the guanidinium ion.

Table 2.2: Relative Gibbs free energies at 298.15K and 1.0 atm in kcal/mol[a]

Configurations	*HF/6-31G**	*B3LYP/6-31G**	*MP2/6-31G**
A	0	0	0
B	-10.5	-15.8	-13.7

[a]Gibbs free energies reported in this table are all relative to those for GdnHCl configuration A, which are -664.132541, -666.114042, and -664.874390 hartrees at the HF/6-31G*, B3LYP/6-31G*, and MP2/6-31G* levels, respectively. The energies were scaled using scale factors described by Scott and Radom.[48]

2.4.10.2 The PS complex

Two models are proposed for the Gdn^+-polypeptide (PS) complexes (Figure 2.15). In model A the side chain represented by methylammonium is positively charged while in model B, the side chain is negatively charged and represented by the acetate ion. In model B, the Gdn^+ interacts directly with both the chloride and acetate anions.
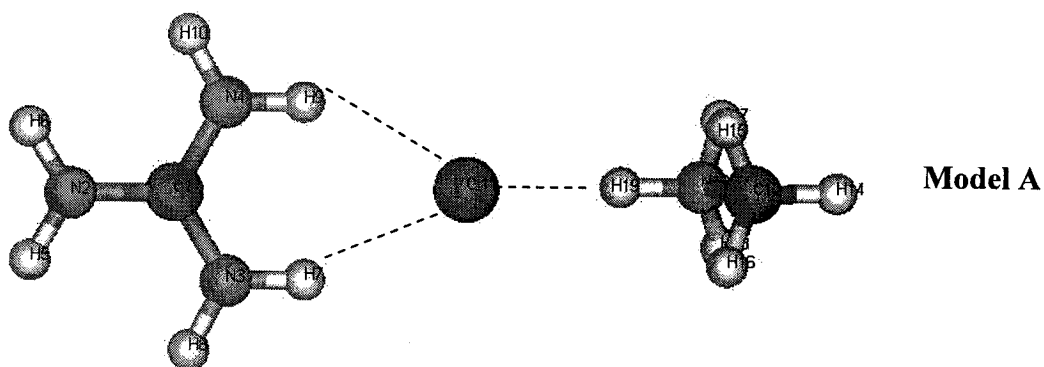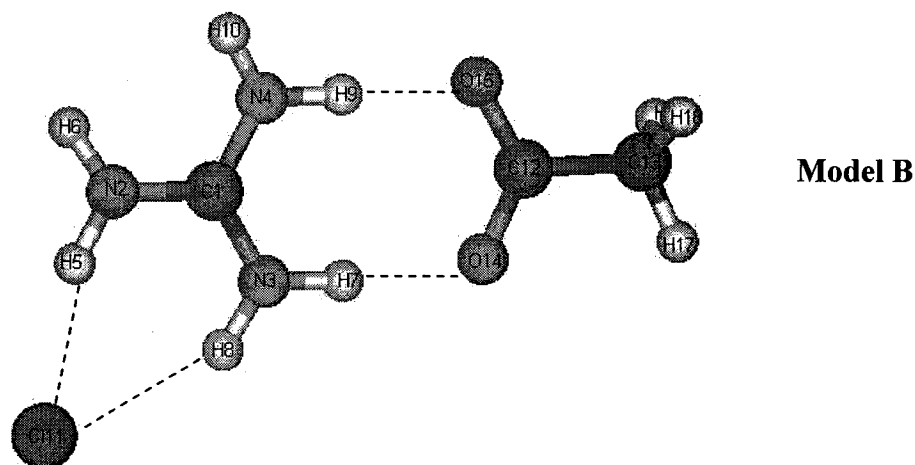
Model A

Model B

Figure 2.15: Two proposed models of the PS complex depending on the charge of the polypeptide side chains. Dashed lines represent weak hydrogen bonds. To reduce computational cost, the positively charged methylammonium ion (model A) and negatively charged acetate ion (model B) are used to represent the side chains of lysine and aspartic acid residues, respectively.

The molecular geometries of Gdn^+, GdnHCl and the PS complex (model A) obtained with HF/6-31G* are illustrated in Figure 2.16. In the absence of the chloride ion, Gdn^+ possesses three equivalent CN bond lengths (1.322 Å). Charge polarization upon addition of the chloride ion results in shortening (0.009Å) of two CN bonds to 1.313Å, and lengthening (0.022 Å) of the third CN bond to 1.344 Å. In the PS complex, the two shorter CN bonds are slightly longer (1.317 Å) than in GdnHCl (1.313 Å), and the third CN bond is shortened (1.331 Å) relative to that in GdnHCl (1.344 Å). Similar results are obtained with B3LYP/6-31G* and MP2/6-31G* calculations except that one of the two CN bond length in PS complex did not change significantly relative to GdnHCl (see Appendices C and D). The CN bond changes in the PS complex relative to GdnHCl are attributed to a lower polarization by the chloride ion in the presence of the positively charged methylammonium. Figure 2.16 also

31

shows that the lengths of the two NH bonds in GdnHCl (1.020 Å) and in the PS complex

(1.006 Å) involved in hydrogen bonding to the chloride increase relative to the others (0.994

Å in GdnHCl and 0.994 Å in PS complex). Similar results were obtained with B3LYP/6-

31G* and MP2/6-31G* model chemistries (see Appendices C and D).

a. Gdn⁺

b. GdnHCl
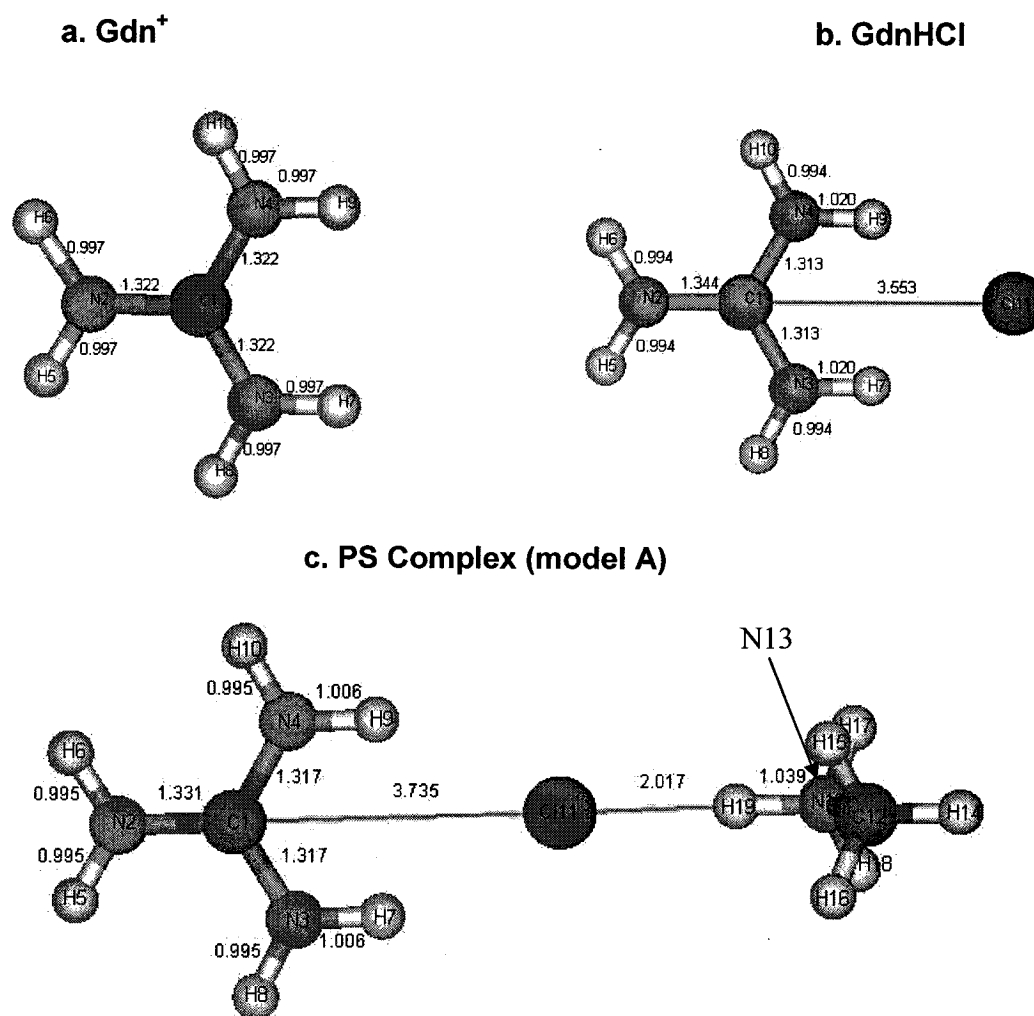
c. PS Complex (model A)

Figure 2.16: Molecular geometries of Gdn⁺, GdnHCl and PS complex model A obtained with the HF/6-31G* model chemistry. All distances are in Angstroms and the C1, N2, N3 and N4 atoms are all in the plane of the paper.

2.4.10.3 NBO analysis of Gdn^+, GdnHCl and PS complex (model A)

A natural bond orbital (NBO) analysis [46, 47] was performed to characterize the nature of the

PS complex. Table 2.3 summarizes the stabilization energies computed from NBO

perturbation theory energy analysis [47] for Gdn^+, GdnHCl and PS complex. The charge

transfer interaction between the lone pairs of nitrogen (n_{N2} and n_{N3}) and the antibonding

orbital of the C1-N4 (π^*_{C1-N4}) is estimated at 119 kcal/mol for Gdn^+. Such high charge

transfer is indicative of resonance stabilization of the Gdn^+ ion. [46, 47]

Table 2.3: Stabilization energies computed from NBO perturbation-theory energy analysis for Gdn^+, GdnHCl and the PS complex (model A) in kcal/mol[a]

Delocalization Interaction	Energy (kcal/mol), Gdn^+	Energy (kcal/mol), GdnHCl	Energy (kcal/mol), PS complex
$n_{N2} \rightarrow \pi^*_{(C1-N4)}$	119	85	106
$n_{N3} \rightarrow \pi^*_{(C1-N4)}$	119	133	127
$n_{Cl11} \rightarrow \sigma^*_{(N3-H7)}$	-	20	5
$n_{Cl11} \rightarrow \sigma^*_{(N4-H9)}$	-	20	5
$n_{Cl11} \rightarrow \sigma^*_{(N13-H19)}$	-	-	45

[a]Stabilization energies for interactions between filled (donor) Lewis-type NBOs and empty (acceptor) non-Lewis NBOs were estimated using 2nd-order perturbation theory analysis of the Fock matrix in the NBO basis for the structures shown in Figure 2.16. [47]

In GdnHCl, the $n_{N2} \rightarrow \pi^*_{C1-N4}$ and $n_{N3} \rightarrow \pi^*_{C1-N4}$ conjugation interaction energies were found to

be 85 kcal/mol and 133 kcal/mol, respectively. Therefore, the presence of the chloride ion

strengthens the $n_{N3} \rightarrow \pi^*_{C1-N4}$ interaction. The reduced $n_{N2} \rightarrow \pi^*_{C1-N4}$ interaction suggest less

delocalization and a longer CN bond (1.344Å) relative to the CN bond (1.322Å) in Gdn^+.

In the PS complex (model A), the $n_{N2} \rightarrow \pi^*_{C1-N4}$ interaction increases to 106 kcal/mol,

suggesting a higher contribution of n_{N2} in the stabilization of the PS complex through

resonance. Thus, the C1-N2 bond should have more double-bond character in the presence of the methylammonium ion. Significant $n_{Cl11}\rightarrow\sigma^*_{N4-H9}$ and $n_{Cl11}\rightarrow\sigma^*_{N3-H7}$ interaction energies of 20 kcal/mol are observed (Table 2.3), indicative of weak hydrogen bonds as previously discussed. In the presence of methylammonium, these interactions are lowered to 5 kcal/mol but a higher $n_{Cl11}\rightarrow\sigma^*_{N13-H19}$ interaction energy (45 kcal/mol) is observed. In the PS complex, the chloride ion interacts strongly with methylammonium and less strongly with Gdn^+ than in GdnHCl.

2.4.10.4 Calculated ν(CN) frequencies in GdnDCl and the PS complex (model A)

Table 2.4 summarizes the calculated values of ν(CN) in GdnDCl and in the PS complex. The two short CN bonds (1.313 Å) in GdnDCl vibrate at a higher wavenumber (v_3) while the single longer CN bond (1.344Å) vibrates (v_1) at a lower wavenumber. The calculated values are in a reasonable agreement with the observed values studied by Venyaminov summarized in Table 2.1. [32] The blue shifts in v_1 predicted by *ab initio* calculations are in reasonable agreement with experimental data (~22 cm^{-1}). Significant (-7 to -12) red shifts in v_3 are also predicted by the model chemistries. A blue shift indicates CN bond strengthening while a red shift indicates a weakening of the CN bond. Close inspection of Figure 2.16c (and Appendices C and D) shows that the CN bond trans to the anion is strengthened while the two CN bonds cis to the anion are weakened or remain unchanged (Appendices C and D) in the PS complex relative to free GdnDCl (Figure 2.16b).

Table 2.4: Calculated ν(CN) frequencies (cm^{-1}) for free GdnDCl and the PS complex (model A)

		GdnDCl	PS complex	$\Delta\nu(CN)^a$
HF/6-31G*	ν_3	1597	1587	-10
	ν_1	1542	1561	19
B3LYP/6-31G*	ν_3	1611	1604	-7
	ν_1	1540	1581	41
MP2/6-31G*	ν_3	1627	1615	-12
	ν_1	1549	1590	41

^{a}Positive values of $\Delta\nu(CN)$ [ν(CN) of PS complex - ν(CN) of free GdnDCl] indicate blue shifts in ν(CN) in the PS complex while negative values indicate red shifts. Here ν_3 is the asymmetric stretch of the short CN bonds in Figure 2.16 (b) and (c), and ν_1 the stretch of the single long CN bond.

2.4.10.5 The PS complex (model B)

Figure 2.17c displays the molecular geometry of the PS complex (model B) predicted by

HF/6-31G*. Here, two negatively charged species, the chloride ion and the acetate ion,

compete for the Gdn^+ ion. Comparison of Figures 2.16b and 2.17 shows that in the presence

of the acetate ion, CN bond shortening occurs from 1.344 Å and 1.313 Å in free GdnHCl to

1.329 Å and 1.307 Å in the PS complex. CN bond shortening is due to the interaction of the

lone pairs of the two oxygens of the acetate ion with antibonding orbitals (π^* $_{C1-N2}$, π^* $_{C1-N4}$)

resulting in more double-bond character in the CN bonds. In addition, bond lengthening in

one of the CN bond occurs from 1.313 Å in free GdnDCl to 1.341 Å in PS complex.

Hydrogen bonds between the acetate ion and the Gdn^+ are also observed as the N2-H6 and

N4-H10 bonds lengthen in the presence of the acetate ion. Table 2.5 summarizes the

calculated frequencies for PS complex (model B). Since, all three CN bonds are inequivalent

in the PS complex in model B (Figure 2.17), *ab initio* calculations predict three different

v(CN). Model B also suggests similar blue and red shifts as observed in Model A.

PS Complex (model B)

Figure 2.17: Molecular geometries of the PS complex obtained with the HF/6-31G* model chemistry. All bond distances are in Angstroms and the C1, N2, N3 and N4 atoms are all in the plane of the paper.

Table 2.5: Calculated v(CN) frequencies (cm^{-1}) for free GdnDCl and in the PS complex (model B)

		GdnDCl	PS complex	$\Delta v(CN)^a$
HF/6-31G*	v_3	1597	1654	57
	v_1	1542	1584	42
	v_2	1597	1530	-67
B3LYP/6-31G*	v_3	1611	1636	25
	v_1	1540	1580	40
	v_2	1611	1520	-91
MP2/6-31G*	v_3	1627	1646	19
	v_1	1549	1582	33
	v_2	1627	1524	-103

[a]Positive values of $\Delta v(CN)$ [v(CN) of PS complex - v(CN) of free GdnDCl] indicate blue shifts in v(CN) in the PS complex while negative values indicate red shifts. v_1, v_2 and v_3 of the PS complex correspond to stretching of the C1-N2, C1-N4 and C1-N3 bonds, respectively in Figure 2.17. Note that v_2 and v_3 are degenerate in GdnDCl and v_1 and v_3 are defined for GdnDCl in the footnote to Table 2.4.

2.5 Discussion

In this work the interaction between Gdn$^+$ and four homopolypeptides was examined. v(CN) of Gdn$^+$ blue-shifts from ~1600 cm^{-1} to ~1622 cm^{-1} upon association with the homopolypeptides. More interestingly, the amide I' band, which is largely due to polypeptide carbonyl stretching does not shift and is relatively unaffected by this interaction. Hence it is proposed that the Gdn$^+$ salts interact with the polypeptide side chains and the role of the anion in the interaction is emphasized. The model proposed involves electrostatic interaction between the Gdn$^+$ salt and the polypeptide side chain groups. The role of the anion depends on the charge of the side chain. For positively charged side chains, the anion acts as a bridge

between the side chain and the Gdn$^+$ cation, whereas for negatively charged side chains, the Gdn$^+$ cation interacts directly with the side chain.

The different interactions of the SCN$^-$ anion with the side chains are reflected in its vibrational frequencies. Different shifts in $\nu(SCN^-)$ are observed in the presence of positively and negatively charged side chains. That is, in the presence of p-Lys and p-Arg, $\nu(SCN^-)$ is red-shifted whereas in the presence of p-Asp it is blue-shifted. In the case of p-Asn, which does not possess a charged side chain, direct charge-dipole interaction of the anion with the side chain and Gdn$^+$ is predicted. Since p-Asn has helical structure, the side chains protrude from the backbone and are exposed to the guanidinium salts. The anion interacts with the amide hydrogen of the side chain, which would explain the red shifted $\nu(SCN^-)$ in the presence of p-Asn (Figure 2.13). In the case of p-Asn, it is possible that the anion interacts with amide hydrogen of the side-chain, which would explain the red-shifted $\nu(SCN^-)$ in the presence of p-Asn (Figure 2.13).

The four homopolypeptides investigated in this work possess polar side chains. It appears that the three guanidinium salts, which include protein denaturants, GdnDCl and GdnDSCN, and the protein stabilizer, $Gdn_2D_2SO_4$, interact in the same manner with the polar polypeptide side chains. It is intriguing that the denaturants and stabilizers behave similarly but there is no obvious reason why $Gdn_2D_2SO_4$ would not interact according to the model proposed in Figure 2.12. The question still remains as to why the SO_4^{2-} salt acts as a stabilizer whereas the Cl$^-$ and SCN$^-$ salts acts as denaturants. Since the interaction of the three guanidinium salts with the polypeptides seem to be similar, the ability of one salt to be a denaturant/stabilizer must depend on other factors. Guanidinium salts, being charged species, are unlikely to

directly interact with the non-polar side chains in proteins and will most probably be excluded from the non-polar surfaces. [7, 15, 16, 49, 50] The ability of a salt to act as a denaturant/stabilizer may be due to the water structure breaking/making properties of the ions specifically at non-polar surfaces.

A comparison of the gas-phase structures of Gdn^+ with GdnHCl (Figure 2.16) demonstrates the importance of polarization effects due to the chloride ion. This ion shortens the two cis CN bonds but shows less effect on the trans CN bond (Figure 2.16). In the presence of methylammonium, the chloride anion interacts less strongly with the Gdn^+ ion, as indicated by the greater Cl-Cl11 bond distance in the PS complex relative to free GdnHCl (Figure 2.16). This results in a larger $n_{N2} \rightarrow \pi^*_{Cl-N4}$ interaction relative to free GdnHCl. Increased delocalization results in strengthening of the C1-N2 bond, which acquires more double-bond character. This explains the blue shifts observed for the C1-N2 bond in the PS complex. The presence of the acetate ion also results in more double-bond character in two of the three CN bonds in model B (Figure 2.17). High delocalization due to the lone pairs of the two oxygens may explain the shortening of the two CN bonds in the PS complex relative to the free GdnHCl (Figure 2.17).

Both models predict significant red shifts in $\nu(CN)$ frequencies upon association. These red shifts are due to lengthening of the CN bonds in the PS complex. Experimentally, red shifting of $\nu(CN)$ was not observed. Since the calculations are performed for gas phase species, it is possible that the addition of water molecules may diminish these red shifts calculated in $\nu(CN)$ by strengthening the CN bonds due to lone pairs of oxygen on water. Therefore,

solvent effects should be included in order to provide a more precise picture of what was observed experimentally.

2.6 Conclusions

We conclude that the interaction of the guanidinium salts with the polar groups of homopolypeptides is similar whether the salt is a kosmotrope or chaotrope. A salt will behave as a denaturant or a stabilizer, based on the water-structure breaking/making properties of the ions. The importance of the solvation in protein folding and the significance of studying the water-structure making/breaking properties of guanidinium salts are emphasized. Interestingly, these salts do not interact with the polypeptide backbone but rather with the polar polypeptide side chains.

CHAPTER 3: THERMAL DENATURATION OF HORSERADISH PEROXIDASE PROBED THROUGH 2D-FTIR, CD AND FLUORESCENCE SPECTROSCOPIES

3.1   Introduction

Horseradish peroxidase isoenzyme C (HRPC) is one of the most studied members of the peroxidase family.[51] It is a monomeric heme-containing plant enzyme of 44kDa that is used to eliminate toxic hydrogen peroxide from the intracellular region.[52] It is stable in aqueous solution and has been used widely in biosensing and biotechnological applications.[52-55] Key residues in the heme cavity are important in regulating the function of HRPC,[52, 56, 57] and comparisons of HRPC and metmyoglobin indicated the importance of these residues in the different reactivity of the two heme proteins towards hydrogen peroxide.[52, 56, 57]

The crystal structure of HRPC has been solved.[58] The enzyme contains two Ca^{2+} binding sites (proximal and distal to heme), four disulfide bridges, N-glycosylation sites and an extensive hydrogen-bonding network.[42, 52, 59] The existence of hydrogen bonding around the heme region is suggested to be a major stabilizing factor in HRPC.[52, 56, 57] The iron of the heme prosthetic group is found to be pentacoordinated.[52] Earlier studies from our laboratory used fluorescence and circular dichorism (CD) spectroscopy to examine unfolding of HRPC and cytochrome c peroxidase (CCP) in denaturants.[60] CCP does not possess disulfide bridges, bound Ca^{2+} or glycosylation sites.[60] Treatment of HRPC with ethylenediaminetetraacetic acid (EDTA) and dithiothreitol (DTT) greatly destabilized HRPC over CCP.[60] Thus, bound Ca^{2+} ions and disulfide bridges present in HRPC increase the stability of HRPC.

Temperature-dependent unfolding of HRPC and CCP was also probed by FTIR in our laboratory.[61] HRPC was found to be more stable than CCP with respect to temperature

denaturation. Moreover, different mechanisms of thermal unfolding were found for HRPC in the Fe(III) and Fe(II) states. The HRPCFe(III) was found to unfold gradually upon heating with global polypeptide unfolding around 90°C without aggregation. The HRPCFe(II) form has a high affinity for CO and forms stable adducts. [61, 62, 63] In HRPCFe(II)CO, bands characteristic of aggregation (1616 cm^{-1} and 1684 cm^{-1}) appeared at 55°C suggesting the beginning of the denaturation. At higher temperatures, these aggregation bands disappeared.

Chattopadhyay and Mazumdar studied the structural and conformational stability of HRPCFe(III) by varying both temperature and pH. [52] Their studies showed melting of the tertiary structure leading to a pre-molten globule intermediate with a T_m value of 45°C at pH 7. At higher temperatures, with a T_m value of 74°C, complete loss of heme from the cavity occurred. The tertiary structure melting was explained by the disruption of the hydrogen bonding network in the heme cavity on protonation of the distal histidine (pK_a of ~5). The CD results indicated the presence of residual helicity at 93°C and a 'high temperature intermediate' was inferred. This latter intermediate was suggested to be stable due to the disulfide bridges in the polypeptide. [52]

3.2 Objective

The objective of this work is to explain the appearance/disappearance of the aggregation bands in HRPCFe(II)CO observed by Holzbaur. [61] Temperature-dependent unfolding of HRPCFe(III) and HRPCFe(II)CO was reexamined by FTIR, CD and fluorescence spectroscopy. In addition, 2D-correlation analysis of the deconvolved FTIR spectra was used to obtain high-resolution information and to determine the differences/similarities in the unfolding pattern of both forms of the HRPC.

3.3 Materials and methods

3.3.1 Materials

Grade I, salt-free, lyophilized horseradish peroxidase (EC 1.11.1.7) was obtained from

Boehringer Mannheim and used without further purification. CO gas (99.3%) was obtained

from Prodair and 99.9% D_2O from Aldrich. All solutions were prepared using distilled water

(specific resistance 18.3Ω) from a Barnstead Nanopure system.

3.3.2 Methods

3.3.2.1 Sample preparation

The samples were dissolved in 100 mM sodium phosphate (NaP_i) buffer at pD 7. The pD

values for buffers prepared in D_2O were calculated from pD = pH(measured) + 0.4.[64] Stock

solutions of HRPCFe(III) were prepared spectrophotometrically using ε_{403}= 102 mM^{-1} cm^{-1}.

[61] Preparation of HRPCFe(II)CO consisted of passing CO gas over 60 μL of HRPCFe(III) in

a sealed Eppendorf tube for ~5 min. Saturated, degassed sodium dithionite (2 μL) in the NaP_i

buffer was added to reduce the ferric heme and the absorption of the CO adduct of

HRPCFe(II) (ε_{422}= 161 mM^{-1} cm^{-1})[61] was monitored spectrophotometrically. The spectra

were recorded on a Hewlett-Packard 8431A UV-visible spectrophotometer.

3.3.2.2 FTIR spectroscopy

FTIR spectra were recorded on a Nicolet FTIR spectrometer equipped with a deuterated

triglycine sulfate (DTGS) detector and purged with dry air from a Balston dryer. The IR cell

consisted of a temperature-controlled cell mount (Model 118-1, Wilmad), two CaF$_2$ windows

(13 x 2 mm) and a 50 μm Teflon spacer (Wilmad). The temperature was controlled to within ±0.5°C by using an Omega thermostat. The sample (15 μL) was then loaded onto one of the CaF$_2$ windows and the cell was immediately assembled and placed into the FTIR cell chamber for spectra recording. To obtain a significant amount of data, an increment of 5°C was used and 15 min of equilibration time was allowed to ensure temperature equilibration before any spectral recording. Each spectrum is an average of 512 scans recorded at a resolution of 4 cm^{-1}. Deconvolution of the amide I' region was performed using the GPLOT software with a K factor of 2 and a resolution (HWHH) of 12.5 cm^{-1} and 15 cm^{-1} for HRPCFe(II)CO and HRPCFe(III), respectively. The concentrations of HRPCFe(III) and HRPCFe(II)CO were determined spectrophotometrically to be 1.13 mM and 2.8 mM, respectively.

3.3.2.3   Two-dimensional correlation analysis

A generalized 2D-FTIR correlation analysis of the deconvolved FTIR spectra was performed as described by Wang.[9] Ranges of 1600-1700 cm^{-1} and 1595-1720 cm^{-1} were chosen for amide I' regions for HRPCFe(II)CO and HRPCFe(III), respectively. Low-temperature (25-65°C) and high-temperature (70-95°C) correlation analyses were carried out for both states of the protein. A 2% correlation intensity cutoff was used to generate the 2D-FTIR plots. The interpretation of these contour plots was carried out as described by Filosa, Wang and Noda.[8, 9, 10]

3.3.2.4   Circular dichroism (CD) spectroscopy of HRPCFe(II)CO at pH 7.0

The CD spectra were recorded on a Jasco J-710 spectrometer purged with N$_2$ at a flow rate of 5 L/min. Spectra of 5.7 μM of HRPCFe(II)CO in 100 mM NaP$_i$ at pH 7 were recorded

between 200 and 300 nm in a 0.1 cm path-length cell at 50 nm/min with a response time of 1 second. The reported spectra are an average of 5 scans at 0.2 nm resolution with a bandwidth of 1 nm.

3.3.2.5   Fluorescence spectroscopy of HRPCFe(II)CO at pH 7.0

Emission spectra (300-400 nm) of 1 μM of HRPCFe(II)CO in 100 mM NaP$_i$ at pH 7 were recorded on a Aminco-Bowman Series 2 luminescence spectrometer following excitation at 295nm to selectively excite tryptophan. [60, 65] The scan rate was 1 nm/s and the slits used were 4 nm.

3.4   Results

3.4.1   FTIR spectroscopy

HRPCFe(III)

The amide I' region can be used to probe the unfolding of different secondary structures in a protein. [1, 61, 66, 67] Figure 3.1 shows the deconvolved spectra of HRPCFe(III) between 25-95°C (Figure 3.1a), 25-60°C (Figure 3.1b), 65-80°C (Figure 3.1c) and 80-95°C (Figure 3.1d). Seven different absorption peaks are identified at 25°C. The 1612 cm^{-1} band is assigned to side-chain vibrations while the 1647 and 1658 cm^{-1} bands are due to different helical structures. The shoulder at 1668 and 1681 cm^{-1} are assigned to loops and turns, respectively. The small shoulder and peak at 1692 and 1703 cm^{-1} are due to β-turns and γ-turns, respectively. These bands are assigned based on the literature assignments. [1,3,61,68] No peak appeared at 1645 cm^{-1} due to random coil structure as we reported previously [61]. At high temperatures, no aggregation bands (1616 cm^{-1} and 1684 cm^{-1}) appeared. Upon increasing the temperature, the intensity of the helical and the side-chain bands decreased while the

absorbance of the loops at 1668 cm^{-1} increased with temperature (Figure 3.1a). Significant

helical structures are observed even at 80°C (Figure 3.1c), consistent with our previous

reports.[61]
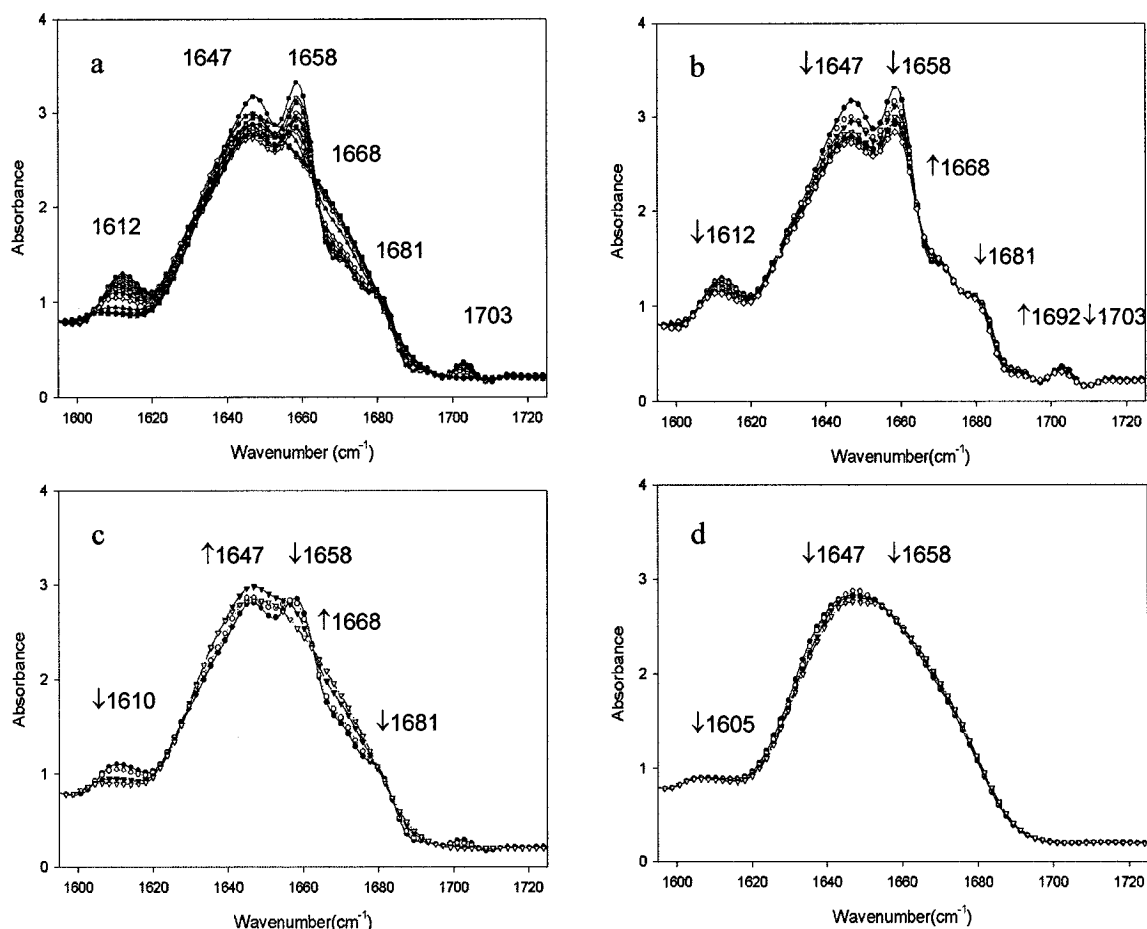
Figure 3.1: Deconvolved spectra in the amide I' region of 2.8 mM HRPCFe(III) in 100 mM phosphate buffer in D_2O at pD 7.0 vs. temperature. (a) 25-95°C, (b) 25-60°C, (c) 65-80°C, and (d) 80-95°C. Each spectrum is the average of 512 scans recorded at 4 cm^{-1} resolution in a 50 μm pathlength cell. Frequencies of the peaks corresponding to different secondary structures are given on the spectra. The up arrows (↑) indicate an increase in intensity while the down arrows (↓) a decrease in intensity with increasing temperature.

Figure 3.2 shows deconvolved FTIR spectra of HRPCFe(III) upon cooling from 95 to 25°C.

Comparison of Figures 3.1 and 3.2 at 25°C reveals that the denaturation is irreversible.

However, Figure 3.2 shows that upon cooling, aggregation bands (1616 and 1684cm^{-1}) appeared at 55°C. This observation was not reported in our previous work.[61]
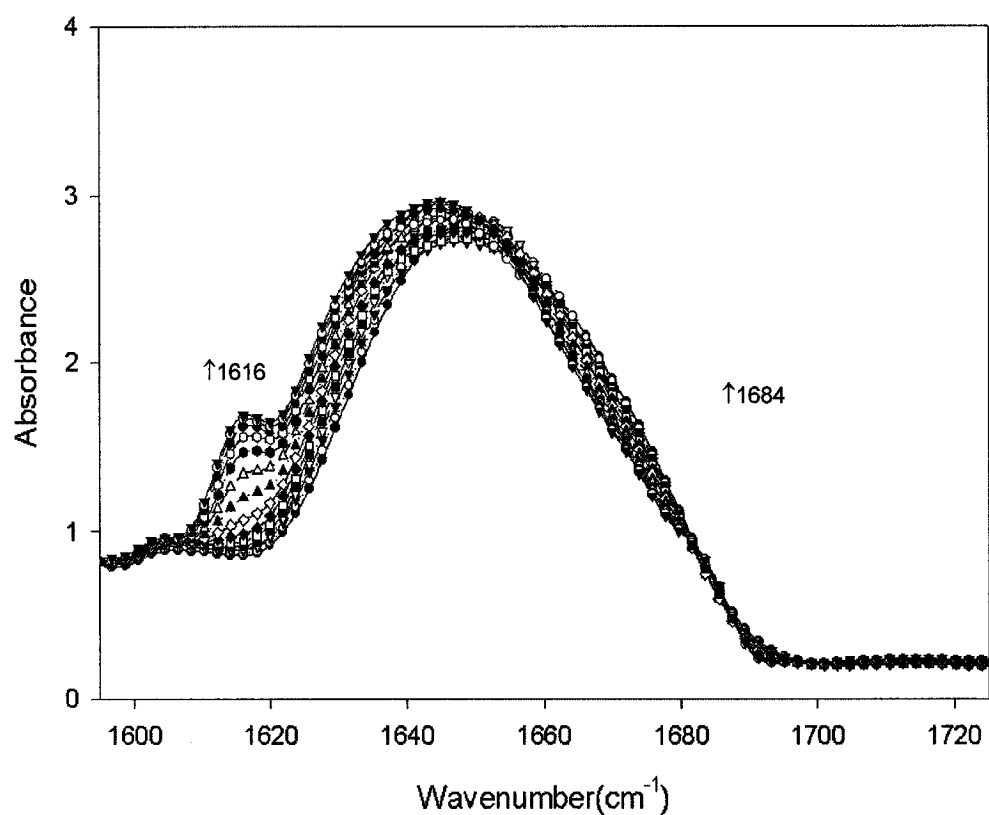
Figure 3.2: Deconvolved spectra in the amide I' region upon cooling 2.8 mM HRPCFe(III) from 95°C to 25°C at pD 7.0. Each spectrum is the average of 512 scans recorded at 4 cm^{-1} resolution in a 50-μm pathlength cell. Frequencies of the peaks corresponding to different secondary structures are given. The up arrows (↑) indicate an increase in intensity while the down arrows (↓) a decrease in intensity with increasing temperature.

Changes in amide II' region can be used to analyze the evolution of the tertiary structure of a protein with increasing temperature. [61,66,1,67,3] In this region, changes in intensity with temperature due to peptide NH/ND exchange are monitored. [61,66,1,67,3] Figure 3.3a shows the changes in the amide II' intensity of HRPCFe(III) upon heating to 95°C. A gradual change in tertiary structure occurs with an increase in temperature up to ~60°C. Between 60 and 80°C complete loss of tertiary structure occurs. Presence of significant secondary structure (Figure 3.1c) and collapsed tertiary structure at 80°C suggests a *pre-molten globule* intermediate.
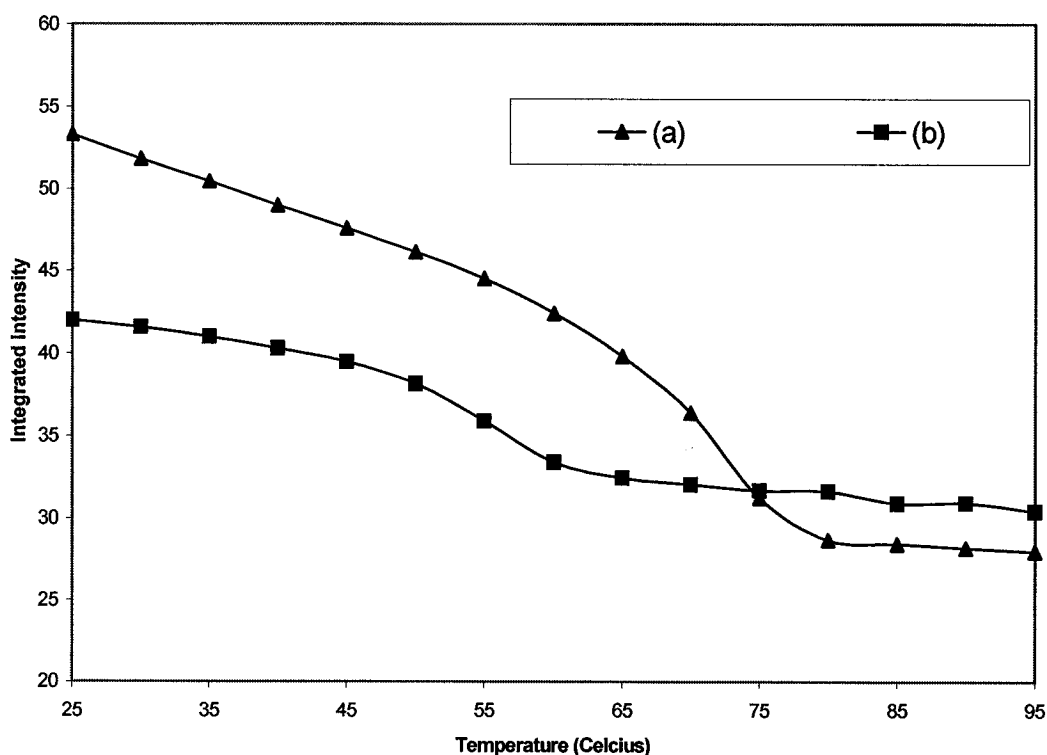
Figure 3.3: Plots of integrated intensities vs. temperature of the amide II' band of HRPC at pD 7.0. (a) 2.8 mM HRPCFe(III) between 1569 and 1521 cm^{-1} and of (b) 1.13 mM HRPCFe(II)CO between 1560 and 1522 cm^{-1}.

HRPCFe(II)CO

The deconvolved amide I' spectra of HRPCFe(II)CO over different temperature ranges are

shown in Figure 3.4. Peaks at 1610, 1648/1658, 1670 and 1684 in Figure 3.4b are assigned to

side-chain vibrations, helical structures, loops and turns, respectively. [61, 66, 1, 67,3] The

aggregation bands at 1615 and 1684 cm⁻¹ appear at 55°C and reach maximum at 65°C

(Figure 3.4c). Above 65°C, the aggregation bands decrease in intensity until 80°C where they

disappear (Figure 3.4d). A dramatic loss in secondary structure occurs above 55°C and a

broad peak centered at 1648cm⁻¹ dominates the spectrum (Figure 3.4c and d).
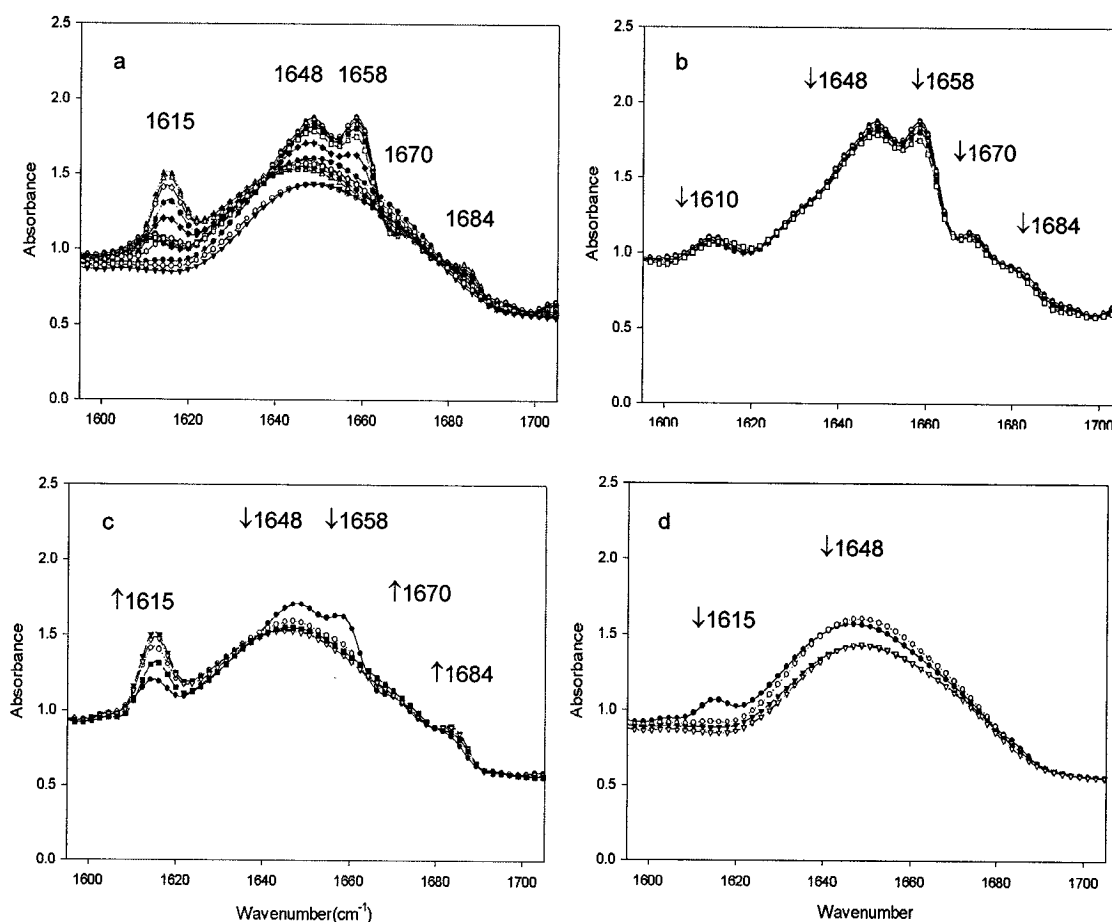
Figure 3.4: Deconvolved spectra vs. temperature in the amide I' region of 1.13 mM
HRPCFe(II)CO in 100 mM sodium phosphate buffer at pD 7.0. (a) 25-95°C, (b) 25-50°C,
(c)55-75°C, and (d) 80-95°C. Each spectrum is the average of 512 scans recorded at 4
cm⁻¹ resolution in a 50 μm pathlength cell. The up arrows (↑) indicate an increase in
intensity while the down arrows (↓) a decrease in intensity with increasing temperature.

Upon cooling, the bands at 1615 and 1684 cm^{-1} reappear indicating the aggregation is reversible (Figure 3.5). On the other hand, loss of secondary structure is irreversible since the spectrum in Figure 3.4 does not resemble the 25°C spectrum in Figure 3.5.This observation is consistent with our published results.[61]
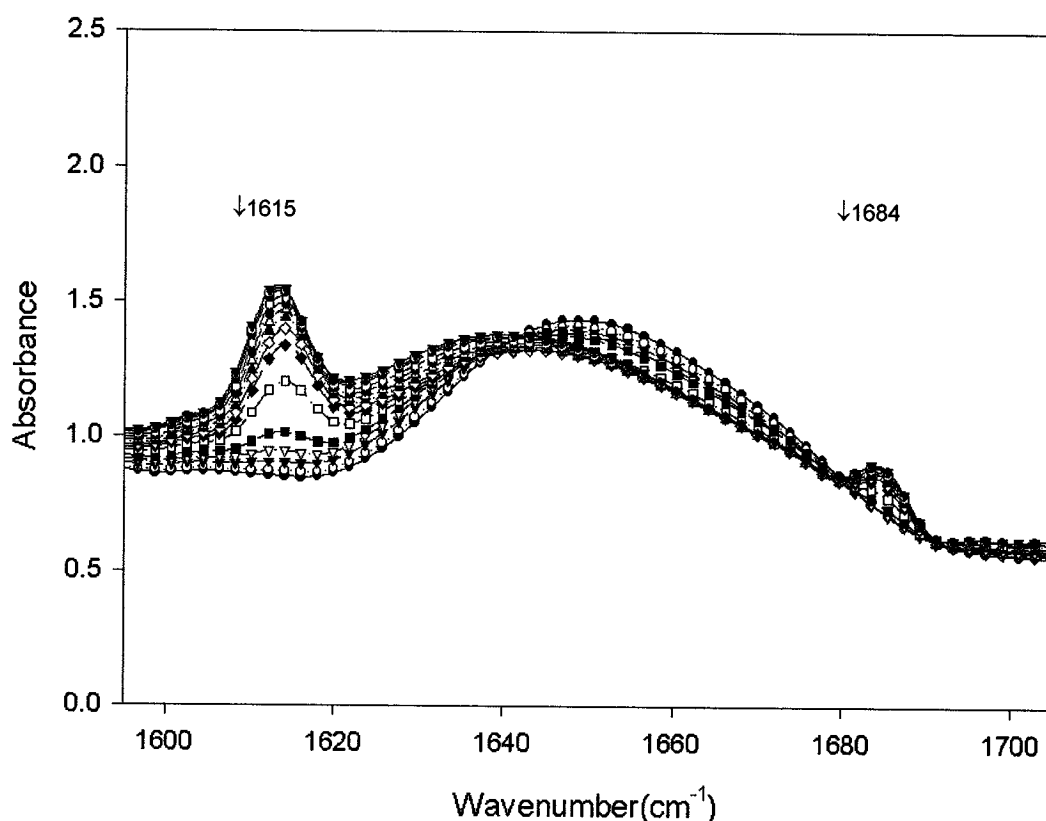
Figure 3.5: Deconvolved spectra in the amide I' region upon cooling of 1.13 mM HRPCFe(II)CO from 95°C to 25°C at pD 7.0. The down arrows (↓) indicate a decrease in intensity with decreasing temperature.

Changes in tertiary structure of HRPCFe(II)CO were also monitored by probing amide II' region. Figure 3.3b shows that HRPCFe(II)CO has lost most of its tertiary structure by 65°C. We previously reported that changes in the amide II' region were similar for the Fe(III) and Fe(II)CO forms of HRPC.[61] Comparison of Figures 3.3a and 3.3b suggests that the global unfolding of HRPCFe(III) occurs at a higher temperature (70 vs. 55°C) than that of

HRPCFe(II)CO consistent with the appearance of high intensity aggregation bands in the

latter (Figure 3.2 vs. Figure 3.5). Changes in the heme pocket can be probed directly by

monitoring $v(CO)$ between 1880 and 1980 cm^{-1}. Two bands at 1901 and 1932 cm^{-1} were

observed at lower temperatures (25 to 55°C) suggesting two different conformations of the

CO ligand in HRPCFe(II)CO. [12] Above 50°C, another peak at 1964 cm^{-1} appears and

increases in intensity with temperature (Figure 3.6) in agreement with our previous results. [61]

The 1901 cm^{-1} band is assigned to $v(CO)$ of a FeCO moiety hydrogen-bonded to a distal

group [61 69 70 71 72] Since both aggregation and 1964 cm^{-1} bands appear at 55°C, the latter was

assigned to $v(CO)$ of denatured HRPCFe(II)CO. [61] The large blue shift in $v(CO)$ on

denaturation is due to heme exposure and interaction of the CO ligand with the negative end

of the dipoles of the aqueous solvent. [70, 73]
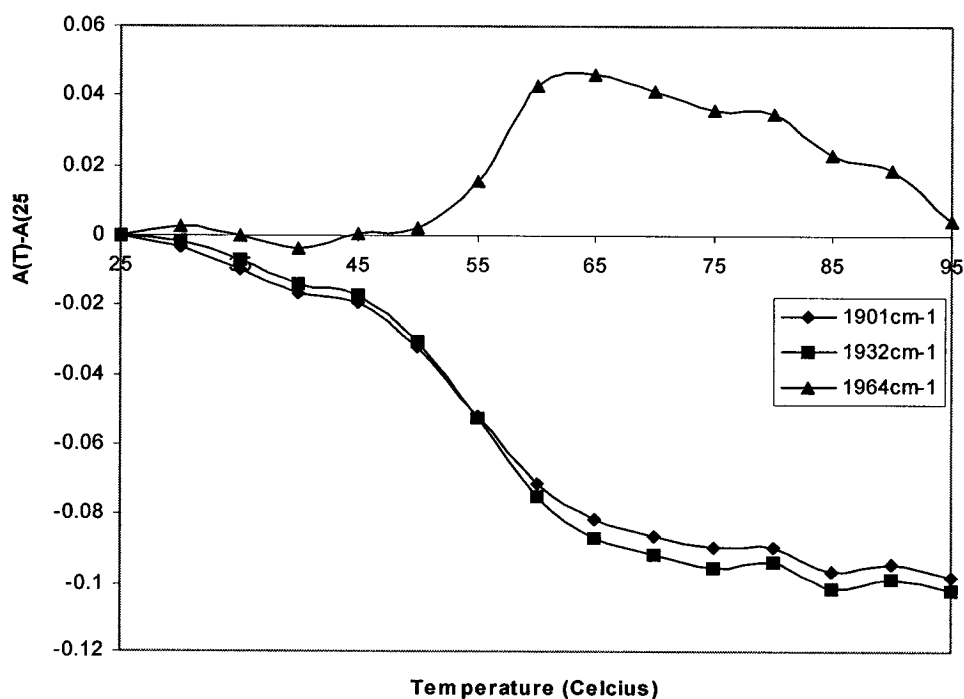
Figure 3.6: Changes in the intensities of $v(CO)$ bands of 1.13 mM HPRCFe(II)CO in 100 mM sodium phosphate buffer at pD 7.0 vs. temperature. The intensities are relative to spectrum at 25°C.

3.4.2 2D correlation analysis

HRPCFe(III)

Figures 3.7a and 3.7b represent synchronous and asynchronous 2D contour plots of the deconvolved spectra of HRPCFe(III) between 25 and 65°C. The auto-peaks along the diagonal line at 1612, 1647 and 1659 cm^{-1} in Figure 3.7a indicate high spectral intensity changes of these bands with temperature. Positive cross-correlation peaks (solid lines) are observed at (X, Z) 1684 vs. 1612cm^{-1}, 1684 vs. 1647cm^{-1} and 1684 vs. 1659 cm^{-1} suggesting that the intensities of the turns, side-chains and helices are changing (decreasing) in the same direction. Positive cross-correlation peaks (X, Z) at 1703 vs. 1647 cm^{-1} and 1703 vs. 1659 cm^{-1} indicate that the γ-turn and helical intensities are also changing in the same direction. Negative cross-correlation peaks (dashed lines) are observed at (X, Z) 1667 vs. 1612 cm^{-1}, 1667 vs. 1647 cm^{-1} and 1667 vs. 1659 cm^{-1} suggesting that loop intensities change in opposite direction to those of the side chains and helices. Other negative cross-correlation peaks (dashed lines) include 1692cm^{-1} vs. 1647 cm^{-1} and 1659 cm^{-1} indicating that β-turn and the helical intensities change in the opposite direction.

Asynchronous (Figure 3.7b) negative cross-correlation peaks are observed at (X, Z) 1684 vs. 1647 cm^{-1} and 1684 vs. 1659 cm^{-1}. In the synchronous plots these frequencies are positively correlated, hence denaturation of the helical structures precedes the turns. Similarly, negative cross-correlation peaks are observed at (X, Z) 1703 vs. 1647 cm^{-1} and 1703 vs. 1659 cm^{-1} in asynchronous plots (Figure 3.7b). In synchronous plots these frequencies are positively correlated, hence denaturation of γ-turns precedes helical structures. Positive cross-correlation peaks are observed at (X, Z) 1667 vs. 1647 cm^{-1} and 1667 vs. 1659 cm^{-1}, which are negative in the synchronous plot and therefore helical denaturation precedes loops

unfolding. The presence of positive cross-correlation peaks at (X, Z) 1659 vs. 1612 cm^{-1},

1647 vs. 1612 cm^{-1} and 1684 vs. 1612 cm^{-1} in both synchronous and asynchronous plots

suggests that the last event between 25 and 65°C in HRPCFe(III) is the change in spectral

intensity due to side-chain vibrations. Table 3.1 summarizes the peak assignments of the 2D

contour plots and the unfolding sequence of the protein between 25 and 65°C.

(a)   *Synchronous 2D Correlation Map*

(b)   *Asynchronous 2D Correlation Map*

Table 3.1: Summary of the peak assignment for the contour plots in Figure 3.7

	1684 ↓	1667 ↑	1659 ↓	1647 ↓
1612 ↓	+ + ←	-	+ + ←	+ + ←
1647 ↓	+ - →	- + →	+ - →	
1659 ↓	+ - →	- + →		
1667 ↑	-			
1647 helix 1659 helix 1667 loops 1684 turns 1612 side chain		⇩		

The signs (+, -) of the X,Z peaks above the diagonal in the 2D synchronous plot (left-hand sign) and the 2D asynchronous plot (right-hand sign) are shown. The vertical arrows indicate an increase (↑) or decrease (↓) in spectral intensity. The horizontal arrows indicate the unfolding sequence of the structural elements (e.g. ← in the first column, first row indicates that the 1684 cm^{-1} band loses intensity before the 1612 cm^{-1} band while → in the second row indicates that the 1647 cm^{-1} band loses intensity before the 1684 cm^{-1} band). The large arrow indicates the overall sequence of unfolding of all structural elements. The table was constructed by following the rules proposed by Noda.[8]

The high temperatures (70 -95°C), synchronous and asynchronous 2D contour plots are shown in Figures 3.8a and 3.8b. The auto-peak at 1686 cm^{-1} (Figure 3.8a) is not observed in Figure 3.7a, which suggests that greater intensity change occurs at 1686 cm^{-1} at higher temperatures. Moreover, the auto-peak at 1612 cm^{-1} is more intense in Figure 3.8a vs. Figure 3.7a suggesting a possible peak at 1615 cm^{-1} is buried underneath. Since aggregation bands tend to appear at 1616 and 1684 cm^{-1}, it is speculated that the buried peak at 1615cm^{-1} is due to aggregation. In addition, upon cooling, the aggregation bands were also observed (Figure 3.2) suggesting reversible aggregation phenomena.

Another auto-peak also appears at ~1638 cm^{-1} in Figure 3.8a indicating that the intensity at 1638 cm^{-1} changes more above than below 70°C. HRPC is known to contain β-sheet structure,[58] which absorb around 1638 cm^{-1}.[3] Autopeaks at 1667 and 1659 cm^{-1} suggest that significant change in loops and helical structures also occur at elevated temperatures as can be seen also in Figure 3.1d. Negative cross-correlation peaks are observed in Figure 3.8a at (X, Z) 1686 vs. 1612 cm^{-1}, 1686 vs. 1647 cm^{-1} and 1686 vs. 1659 cm^{-1} suggesting that side-chain and helical intensity changes occur in the opposite direction relative to the aggregation band. Negative cross-correlation peaks at (X, Z) 1667 vs. 1612 cm^{-1}, 1667 vs. 1647 cm^{-1} and 1667 vs. 1659 cm^{-1} indicate opposite intensity change of the loop relative to the side-chain and helical structures. A negative cross-correlation peak suggests that the intensity at (X, Z) 1667 and 1686 cm^{-1} increases with temperature while helical bands decrease in intensity. Negative cross-correlation peaks in both Figure 3.8a and 3.8b are seen at (X, Z) 1686 vs. 1647 cm^{-1} and 1667 vs. 1647 cm^{-1} and suggest that aggregation bands and loops unfold prior to helixes (1647 cm^{-1}). Positive cross-correlation peaks in Figure 3.8a and 3.8b at (X, Z) 1659 vs. 1647 cm^{-1} indicate that 1659 cm^{-1} helix unfolds prior to 1647 cm^{-1} helix. Close inspection of Figures 3.8a and 3.8b reveals that, at high temperature (70-95°C), change in side-chain intensity is followed by the unfolding of secondary structure as follows: aggregation (1686) < helix (1659) < loops (1667) < helix (1647) where the sign "<" indicate "precedes". Table 3.2 summarizes the peak assignments of the 2D FTIR maps of Figures 3.8a and 3.8b.
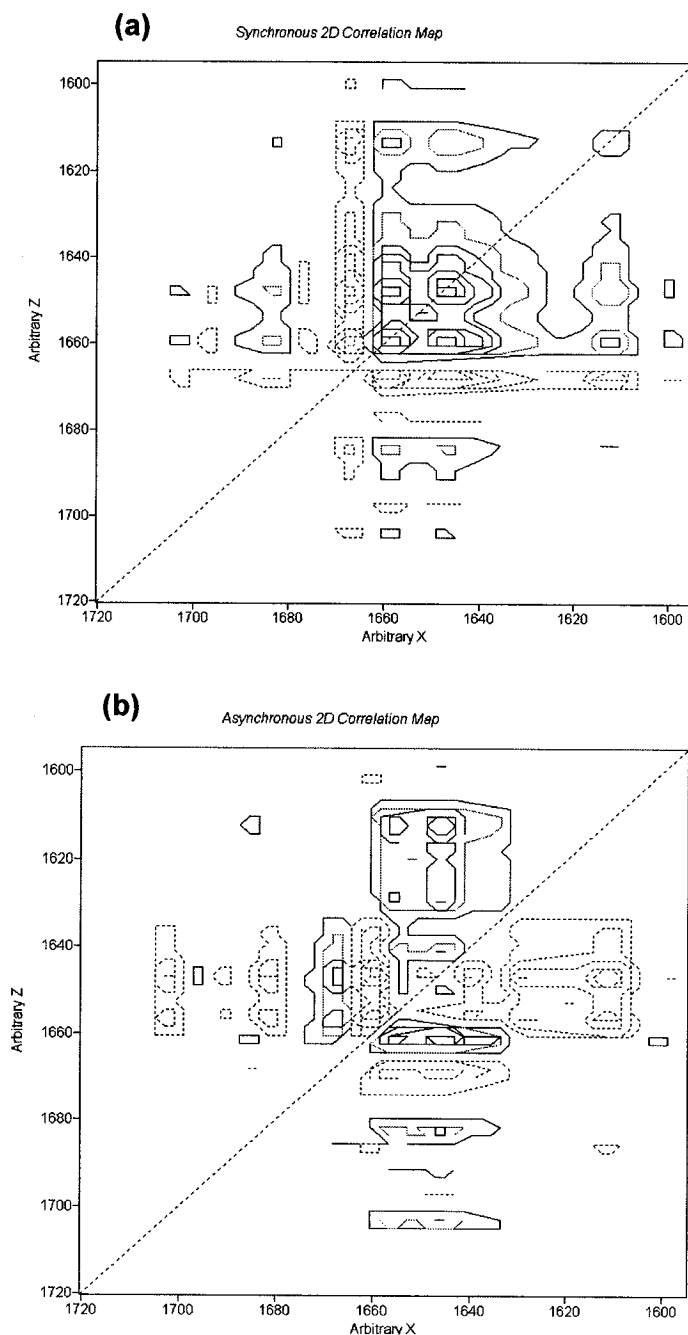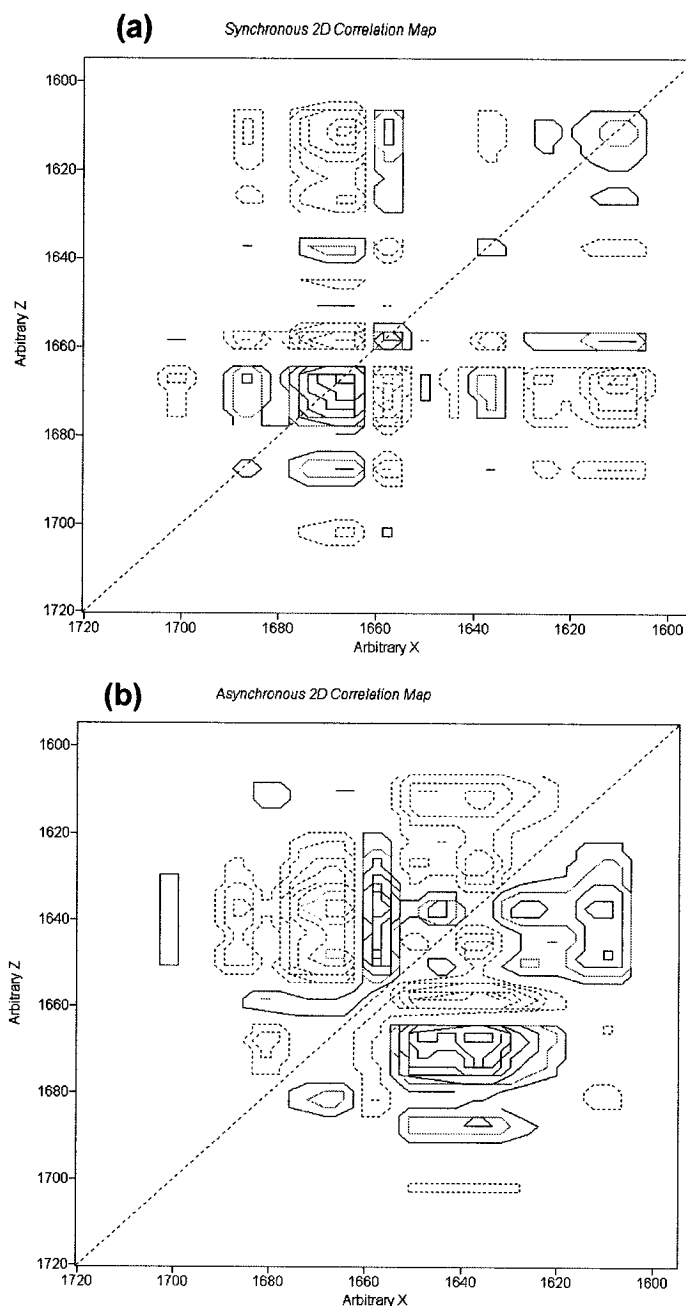
Figure 3.8: 2D FTIR (a) synchronous and (b) asynchronous contour plots of the amide I' region of HRPCFe(III) at 70-95 °C. The plots are constructed from the FTIR data in Figure 3.1 between 70 and 95°C using Grams 2D software.[9] Solid and dashed lines represent positive and negative correlation peaks, respectively.

Table 3.2: Summary of the peak assignments for the contour plots in Figure 3.8

	1686 ↑	1667 ↑	1659 ↓	1647 ↓
1612 ↓	-	-	+	+ - →
1647 ↓	- - ←	- - ←	+ + ←	
1659 ↓	- →	- + →		
1667 ↑	+			
1612 side chain 1686 aggregation 1659 helix 1667 turns 1647 helix		⇓		

The signs (+, -) of the X, Z peaks above the diagonal in 2D synchronous plot (left-hand sign) and 2D asynchronous plot (right-hand sign) are shown. The horizontal and vertical arrows are as described in Table 3.1. The unfolding sequence of secondary structures is shown by the large at the bottom of the table. The table was constructed by following the rules proposed by Noda.[8]

HRPCFe(II)CO

Figure 3.9a and 3.9b show synchronous and asynchronous contour plots of HRPCFe(II)CO between 25-65°C. Auto-peaks at 1615, 1648 and 1658 cm^{-1} are observed indicating greater changes for these structures relative to loops (Figure 3.9a). Negative cross-correlation peaks at (X, Z) 1670 vs. 1615 cm^{-1}, 1658 vs. 1615 cm^{-1} and 1648 vs. 1615 cm^{-1} in both Figures 3.9a and 3.9b suggest that the unfolding of loops and helical structures precedes aggregation whereas positive cross-correlation peaks at (X, Z) 1670 vs. 1648 cm^{-1} and 1670 vs. 1658 cm^{-1} in both figures indicate that the loops unfold prior to helical structures. A positive cross-correlation peak in Figures 3.9a and 3.9b at (X, Z) 1658 vs. 1648 cm^{-1} suggests that unfolding of 1658 cm^{-1} helix precedes that of the 1648 cm^{-1} helix. Negative and positive cross-correlation peaks at (X, Z) 1684 vs. 1670 cm^{-1} in Figures 3.9a and 3.9b, respectively, suggest that the aggregation (1684 cm^{-1}) is the last event to occur between 25-65°C.

Figure 3.9: 2D FTIR (a) synchronous and (b) asynchronous contour plots of the amide I' region of HRPCFe(II)CO at 25-65 °C. The plots were constructed from the FTIR data in Figure 3.4 between 25 and 65°C using Grams 2D software. [9] Solid and dashed lines represent positive and negative correlation peaks, respectively.

Table 3.3: Summary of the peak assignments for the contour plots in Figure 3.9

	1684 ↑	1670 ↓	1658 ↓	1648 ↓
1615 ↑	+ - →	- - ←	- - ←	- - ←
1648 ↓	- + →	+ + ←	+ + ←	
1658 ↓	- + →	+ +		
1670 ↓	- + →			
1670 turns 1658 helix 1648 helix 1615 aggregation 1684 aggregation	⇩			

The signs (+, -) of the X,Z peaks above the diagonal in 2D synchronous plot (left-hand sign) and 2D asynchronous plot (right-hand sign) are shown. The horizontal and vertical arrows are as described in Table 3.1. The large arrow at the bottom of the table shows the unfolding sequence of secondary structures. The table was constructed by following the rules proposed by Noda.[8]

At high temperatures (70-95°C) unfolding of turns (1670 cm^{-1}) and helices (1659 cm^{-1}) preceded protein aggregation (1615 and 1684cm^{-1}) followed by the changes in the 1648 cm^{-1} helix as seen in Figures 3.10a and 3.10b. It is unlikely that the band at 1648 cm^{-1}, observed in Figure 3.1d and 3.4d, is due to random coil absorption since CD spectroscopy shows significant amount of helical structures at high temperatures (discussed below). Table 3.3 and 3.4 summarize the intensity changes observed in the contour plots in Figures 3.9 and 3.10, respectively.

(a) Synchronous 2D Correlation Map
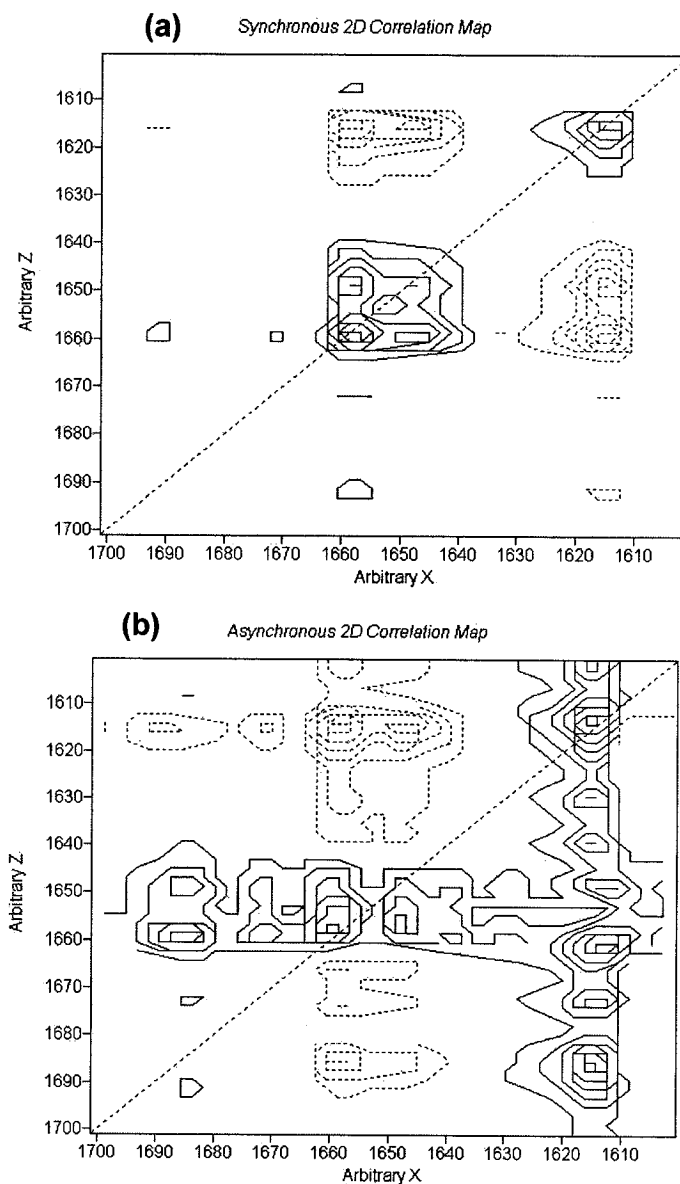
(b) Asynchronous 2D Correlation Map
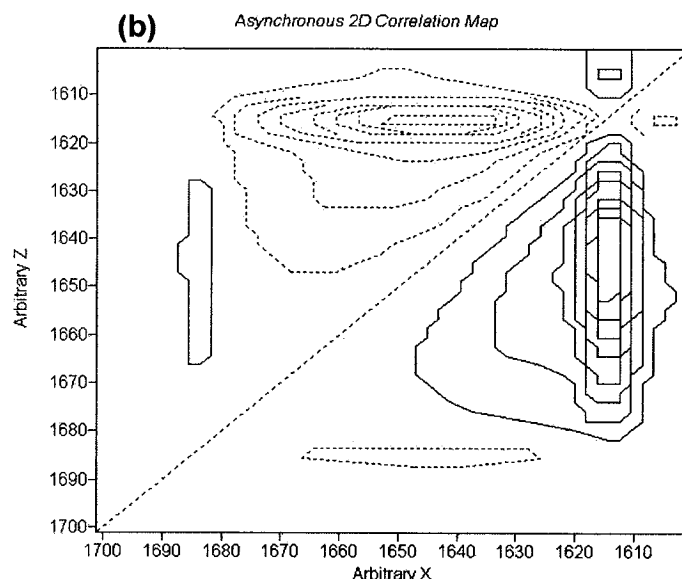
Figure 3.10: 2D FTIR (a) synchronous and (b) asynchronous contour plots of the amide I'
region of HRPCFe(II)CO at 70-95 °C. The plots were constructed from the FTIR data in
Figure 3.4 between 70 and 95°C using Grams 2D software.[9] Solid and dashed lines represent
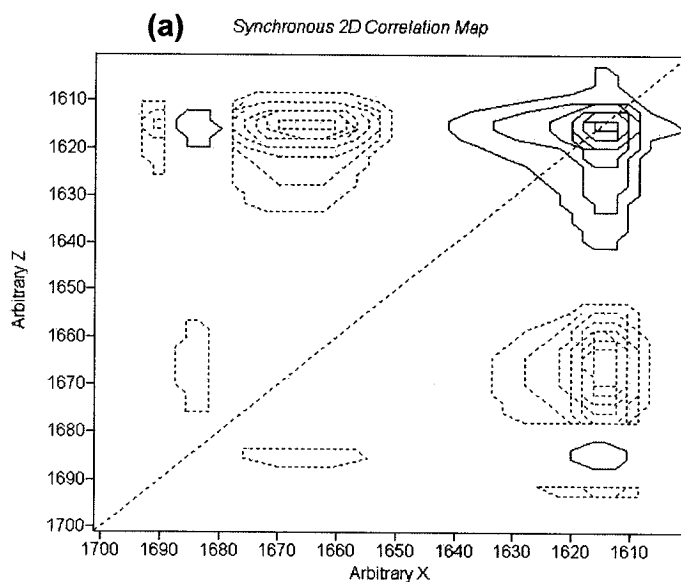positive and negative correlation peaks, respectively.

Table 3.4: Summary of the peak assignments for the contour plots in Figure 3.10

	1684 ↓	1670 ↑	1659 ↑	1648 ↓
1615 ↓	+ ~	- - ←	- - ←	+ - →
1648 ↓	+ + ←	- - ←	- - ←	
1659 ↑	- + →	+ ~		
1670 ↑	- + →			
1670 turns 1659 helix 1615 aggregation 1684 aggregation 1648 helix		⇩		

The signs (+, -) of the X,Z peaks above the diagonal in 2D synchronous plot (left-hand sign)
and 2D asynchronous plot (right-hand sign) are shown. The horizontal and vertical arrows are
as described in Table 3.1. The large arrow at the bottom of the table shows the unfolding
sequence of secondary structures. The table was constructed by following the rules proposed
by Noda.[8]

3.4.3 CD spectroscopy

HRPCFe(II)CO

The thermal unfolding of HRPCFe(II)CO was monitored by CD at 222nm.[74] Figure 3.11 shows the change in ellipticitiy at 222nm with temperature. Spectra beyond 80°C were not obtained due to reliability of temperature controller beyond 80°C. Nevertheless, Figure 3.11 shows that even at 80°C, there is residual absorption at 222nm suggesting that complete loss of helical structures has not occurred. The unfolding of helical structures begins at 55°C (Figure 3.11), which coincides with the onset of aggregation (Figure 3.4c) and continues to 80°C where the aggregation bands disappear (Figure 3.4d).

Figure 3.11: The observed ellipticity vs. temperature of 5.7 μM HRPCFe(II)CO in sodium phosphate buffer at pH 7.0 as probed by CD spectroscopy at 222 nm.The pathlength used was 0.1 cm at a speed of 50 nm/min with response time of 1 s.

3.4.4 Fluorescence spectroscopy

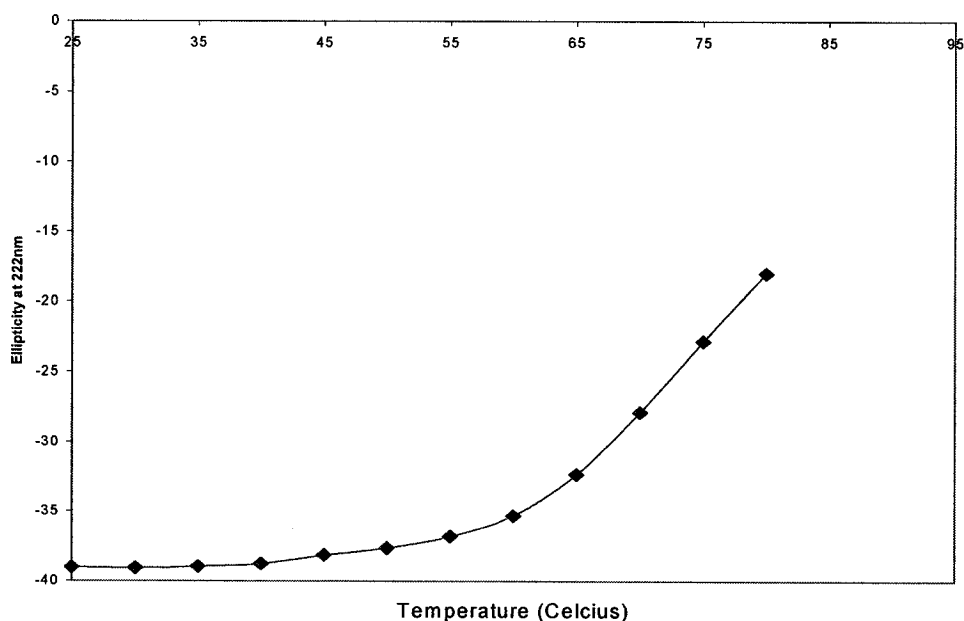Intrinsic fluorescence of heme proteins is dependent on energy transfer from the tryptophan

and tyrosine residues. [75, 76, 77, 78] Unfolding of the protein results in increasing the distance

between the fluorophores and the heme, thereby decreasing the quenching effect of the heme.

Fluorescence intensity should therefore increase in the unfolded protein. [52, 59] Moreover, a red

shift in fluorescence maximum is generally an indication that tryptophan is in a more polar

environment in the unfolded form. [52, 79] HRPC has one tryptophan (Trp117) and five

tyrosines. [52, 58]

HRPCFe(II)CO

The fluorescence emission spectra of HRPCFe(II)CO upon excitation at 295 nm are shown in

Figure 3.12. The integrated intensity between 300 and 400 nm vs. temperature is plotted in

Figure 3.13. The first transition observed in Figure 3.13 (30-40°C, T_m ~35°C) corresponds to

a local change in conformation around heme while the second transition (45-55°C, T_m

~50°C) is accompanied by a sharp increase in fluorescence intensity due to loss of heme. The

third transition (60-70°C, T_m ~ 65°C) coincides with the loss of aggregation bands (Figure

3.4) and loss of tertiary structure (Figure 3.3b). It is likely that complete loss of heme does

not occur until 70°C since the fluorescence intensity continues to rise until 70°C. After 75°C,

a dramatic decrease in fluorescence intensity occurs suggesting major conformational change

in the protein at these temperatures. Tryptophan fluorescence may decrease with temperature

although here we observe drastic reduction in intensity. Also, a decrease in 1964 cm^{-1} FTIR

band at temperatures above 65°C (Figure 3.6) again suggests change in protein conformation.

It is possible that at temperatures above 70°C, disruption of weak intermolecular bonds

(aggregation) reduces fluorescence intensity due to quenching by the solvent and/or heme.
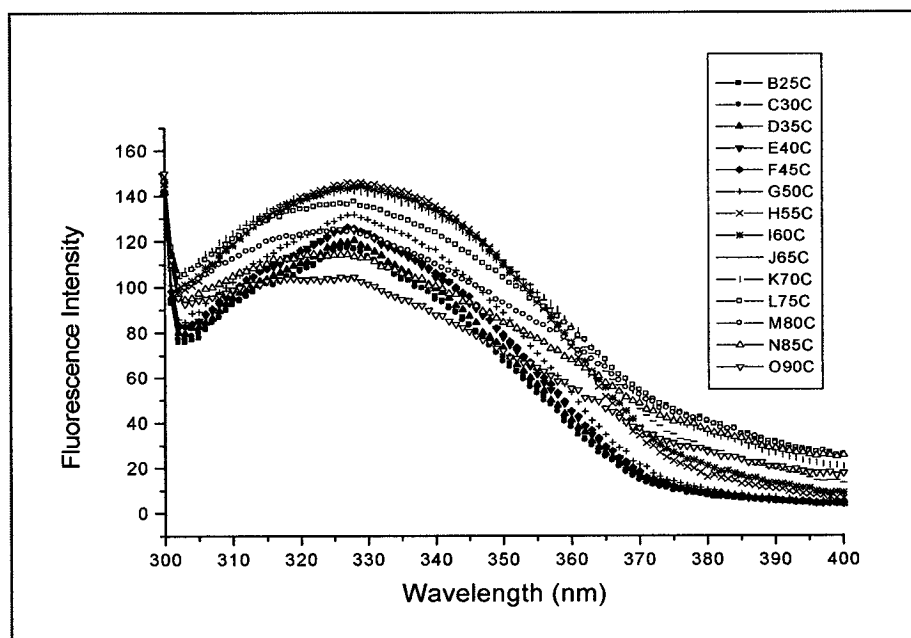
Figure 3.12: Fluorescence emission spectra of 1 μM HRPCFe(II)CO in 100 mM sodium phosphate buffer at pH 7.0 between 25 and 90°C. The excitation wavelength was 295nm.
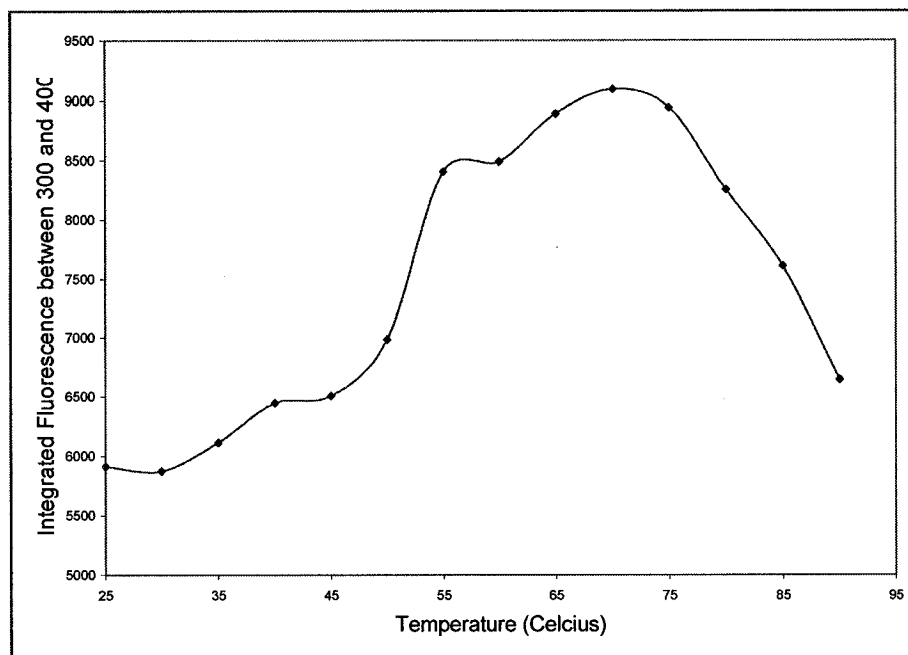

Figure 3.13: Change in integrated fluorescence intensity between 300 and 400 nm vs. temperature of 1 μM HRPCFe(II)CO at pH 7.0. Data are from Figure 3.12.

3.5   Discussion

Thermal denaturation of both HRPCFe(III) and HRPCFe(II)CO is irreversible upon heating to 95°C. HRPCFe(III) is more stable than HRPCFe(II)CO since the tertiary structure of the former is lost at 80°C while that of the latter at 65°C. In addition, intense aggregation bands appear at 55°C in HRPCFe(II)CO whereas weak aggregation bands (only visible with 2D correlation analysis) appear at high temperature (70 -95°C) in HRPCFe(III).

The binding of Ca^{2+} ions, the disulfide bridges and the extensive hydrogen bonding network in the heme cavity are key stabilizing elements in HRPC. [52, 61] Previously we reported that the unfolding of the tertiary structure of both HRPCFe(III) and HRPCFe(II)CO was similar. [61] However, in this work it was found that the global unfolding of HRPCFe(III) occurs at higher temperatures than that of HRPCFe(II)CO (Figure 3.3). Since, over two-fold excess of sodium dithionite was added in this work compared to our previous work, it is speculated that the sodium dithionite not only reduced the Fe(III) heme but also some of the disulfide bridges. Cleavage of disulfide bridges would result in destabilization of the protein. [52, 61] Treatment of HRPCFe(III) with 30 mM dithiothreitol (DTT) lowered the T_m of unfolding from 74 to 65°C and no residual helicity was observed at high temperature. [52] The fact that at 80°C, CD spectroscopy showed presence of residual helical structures in HRPCFe(III) (Figure 3.11) further suggests that the lower stability of the tertiary structure of HRPCFe(II)CO observed in this work is due to partial reduction of the disulfide bridges.

Proteins with helical structures show a signal at 222nm in their CD spectroscopy. [74] Chattopadhyay and Mazumdar studied the effect of temperature on the α-helical absorption of HRPCFe(III) at 222nm. [52] A two-state melting of secondary structure of HRPCFe(III) was

found with T_m value of 74°C. However, HRPCFe(III) still contained secondary structure at

93°C when compared to CD spectrum of HRPCFe(III) in 6M guanidine hydrochloride

(GdnHCl). [52] In addition, the effect of increasing temperature on the structure of

HRPCFe(III) around heme was monitored by Soret-CD at 407nm. [52] Two distinct phases

were observed; the first phase (between 35 and 55°C) was associated with a change in local

conformation of the heme active site and the second phase (between 65 and 85°C) with heme

loss from the active site. Thus, thermally induced unfolding of the HRPCFe(III) proceeds via

an intermediate which is related to a pre-molten globule folding intermediate, which appears

after the first phase of unfolding. [52]

Previously our laboratory showed that HRPCFe(III) did not aggregate at higher temperatures

while HRPCFe(II)CO did. [61] In this work, 2D correlation spectroscopy revealed the presence

of aggregation bands in HRPCFe(III). However, the intensities of the aggregation bands are

higher in HRPCFe(II)CO relative to those of HRPCFe(III) (Figure 3.8a vs. Figure 3.10a).

Changes in the v(CO) in the heme pocket (Figure 3.6) show that denaturation of

HRPCFe(II)CO begins at ~55°C and continues until 65°C as seen by the increase in the

intensity of 1964cm^{-1} peak. These changes are consistent with the changes in the intensity of

aggregation bands, which also begin at 55°C and reach a maximum at 65°C. It is therefore

speculated that the aggregation bands appear due to disruption of the hydrogen-bonding

network within the heme pocket. Reduction of Fe(III) to Fe(II) disrupts this network resulting

in the high-intensity aggregation bands. However, above 65°C, the aggregation bands in

HRPCFe(II)CO start to decrease in intensity and they disappear above 80°C. It is unclear

why this occurs. A possible explanation is that the higher temperatures disrupt the

intermolecular bonds in HRPCFe(II)CO and promote intramolecular bonding, which results

in conformational change in HRPCFe(II)CO. The presence of these intramolecular bonds may explain the presence of significant helical structures even at 80°C in CD spectroscopy. The fluorescence studies of the thermal denaturation by Chattpadhyay and Mazumdar show biphasic unfolding of HRPCFe(III) with T_m values of 42 and 72°C. [52] Similar biphasic unfolding was observed by monitoring the Soret-CD absorption at 407nm. [52] They proposed that the thermal unfolding pathway of HRPCFe(III) followed the sequence N→U'→U"→U. The first intermediate (U') has intact secondary structure but altered tertiary structure in the heme cavity due to changes in the hydrogen-bonding network involving the distal histidine (*pre-molten globule intermediate*). [52] Formation of the second intermediate (U") was associated with cleavage of the Fe-His proximal bond and loss of the heme. [52] In this work, the fluorescence-monitored (295 nm) thermal unfolding of HRPCFe(II)CO shows similar trends as that of HRPCFe(III). The first phase of unfolding of HRPCFe(II)CO occurred between 30 and 40°C (T_m =35°C) and the second phase between 45 and 70°C (T_m = 60°C) as shown in Figure 3.13. It is speculated that both of these phases are due to changes proposed for HRPCFe(III). [52] A dramatic increase in fluorescence intensity occurs between 45 and 54°C and another increase between 60 and 70°C. An increase in fluorescence intensity suggests that the distance between typtophan and the heme is increasing, an indication of loss of heme. However, between 54 and 60°C the fluorescence intensity remains unaltered suggesting a possibility of another intermediate although more data may be required to support this idea. Above 75°C, there is a dramatic decrease in fluorescence intensity, which may be due to changes in protein conformation and to decrease in tryptophan fluorescence intensity. The fact that 1964 cm^{-1} band also decreases above 65°C indicates loss of aggregation and rearrangement in protein structure.

The 2D-correlation analysis revealed the presence of aggregation bands in HRPCFe(III)

(Figure 3.8) as well as in HRPCFe(II)CO. The sequence of unfolding of the secondary

structures of HRPC was also obtained as summarized for HRPCFe(III) and HRPCFe(II)CO

in Tables 3.1 to 3.4. The unfolding of the loops (1670 cm^{-1}) is the first event in

HRPCFe(II)CO while in HRPCFe(III) the helices unfold prior to the loops between 25 and

65°C. Therefore, reduction of Fe(III) to Fe(II) and binding of CO results in destabilization of

loop structures in HRPC. A possible explanation may be that reduction disturbs the

hydrogen-bonding network thereby stabilizing the helices and destabilizing the loops.

Moreover, partial reduction of the disulfide bridges may alter the stability of the helices. In

addition, the 2D-correlation analysis shows that both HRPCFe(III) and HRPCFe(II)CO

unfold in a cooperative manner. An interesting example of cooperation is observed between

helices that absorb at different frequencies. Between 25 and 65°C, it was found that the 1658

cm^{-1} α-helix starts to unfold at lower temperature compared to the 1648 cm^{-1} α-helix in

HRPCFe(II)CO. On the other hand, in HRPCFe(III), the 1648 cm^{-1} helix unfolds prior to the

1658 cm^{-1} helix.

3.6 Conclusions

Aggregation bands (1616 and 1684 cm^{-1}) and the unfolding of tertiary structure was observed at lower temperatures in HRPCFe(II)CO than in HRPCFe(III) suggesting higher stability of the latter. It is speculated that reduction of Fe(III) to Fe(II) causes a disruption of the hydrogen-bonding network resulting in the greater aggregation of HRPCFe(II)CO relative to HRPCFe(III). At temperatures above 65°C, the weak intermolecular interactions involved in HRPCFe(II)CO aggregation are possibly broken since the FTIR aggregation bands decrease in intensity and disappear at 80°C . On the other hand, breaking of these weak intermolecular bonds is possibly counterbalanced by the formation of weak intramolecular bonds since CD spectroscopy shows presence of helical content even at 80°C.

Addition of excess sodium dithionite in this work resulted in the unfolding of the HRPCFe(II)CO tertiary structure at lower temperature (55°C) than we previously reported (≈55°C). [61] It is speculated that the excess sodium dithionite not only reduced Fe(III) but also some of the disulfide bridges. Since a high content of helical structure still exists at 80°C, only partial reduction of the four disulfide bridges is predicted.

The high-resolution 2D-correlation analysis has been useful since aggregation bands were observed for HRPCFe(III). From the sequence of unfolding, it was found that the reduction of Fe(III) to Fe(II) in HRPC stabilizes/destabilizes certain secondary structures and the sequence are different for the two forms. Moreover, in both forms, the unfolding occurs in highly cooperative manner as the unfolding of a certain structure is dependent upon unfolding of the other structure.

CHAPTER 4: GENERAL CONCLUSIONS AND FUTURE STUDIES

This work has shown the use of spectroscopy and molecular modeling in studying important scientific problems. FTIR difference spectroscopy is a powerful technique in investigating molecular-level interactions between GdnX salts and homopolypeptides. Computational methods were useful in supporting the experimental data and in suggesting the importance of the water-structure making/breaking properties of salts. Guanidinium salts were shown to interact similarly with the polar homopolypeptides in this study. The salts interact with the polypeptide side chains whereas the polypeptide backbone remained unaffected by this interaction. This work suggests that the classification of a salt as a protein stabilizer or denaturant depends on how it interacts with the nonpolar residues in a protein. Specifically, it depends on how the salt makes/breaks the water structure around the nonpolar residues. An interesting study would be to look at the structure of water around each salt ion in this study by using semi-empirical/molecular dynamics simulation.

The 2D-correlation analysis was useful in providing high-resolution data and in suggesting the sequence of unfolding of various secondary structures in two forms of HRPC. We were able to deduce the cooperative unfolding of HRPC since successive unfolding of the structure occurred. Fluorescence studies determined different phases of unfolding of HRPC and indicated the presence of intermediates. CD spectroscopy was also invaluable in supporting the data obtained through FTIR and fluorescence. Further experiments using these tools could provide more insight in the stability of these proteins. For example, the effect of pH on HRPCFe(II)CO at different temperatures and the Soret-CD of this protein could give more information about the heme region and explain how some residues (such as histidine) could be affected by pH and temperature. In addition, site directed mutagenesis of key residues

involved in the hydrogen-bonding network in the heme region should increase our understanding of the unfolding pathway of HRPC. It would be interesting to know which residues in HRPC are involved in aggregation and why aggregation is lost at high temperatures since this phenomenon is not common to many proteins.

REFERENCES

1.   Susi, H., and Byler, D.M., *Methods in Enzymol.*, **1986**. **130**: p. 290-311.

2.   Surewicz, W.K., and Mantsch, H.H., *Biochem. Biophys. Acta.*, **1988**. **952**: p. 115-130.

3.   Haris, P.I., and Chapman, D., *Biopolymers*, **1995**. **37**: p. 251-263.

4.   Jackson, M., and Mantsch, H.H., *Can. J. Chem.*, **1991**. **69**: p. 1639-1642.

5.   Jackson, M., and Mantsch, H.H., *Crit. Rev. Biochem. Mol. Biol.*, **1995**. **30**: p. 95-120.

6.   Dong, A., Huang, P., and Caughney, W.S., *Biochemistry*, **1990**. **29**: p. 3303-3308.

7.   Creighton, T.E., in Protein Structure: A Practical Approach, 2nd edition, Oxford; New York: IRL press at Oxford University Press, NY, **1997**.

8.   Noda, I., *Appl. Spectrosc*, **1993**. *47*: p. 1329-1336.

9.   Wang, Y., Murayama, K., Myojo, Y., Tsenkova, R. , Hayashi, N., and Ozaki, Y., *J. Phys. Chem. B*, **1998**. *102*: p. 6655-6662.

10.   Filosa, A., Wang, Y., Ismail, A.A., and English A.M., *Biochemistry*, **2001**. *40*: p. 8256-8263.

11.   Meyers, R.A., in Circular Dichroism in Protein Analysis (Price, N.C., Ed.), VCH Publishers Inc., New York, **1995**.

12.   Fox, T., Ferreira-Rajabi, L., Hill, B.C., and English, A.M., Biochemistry, **1993**. **32**: p. 6938-6943.

13.   Das, T.K.and Mazumdar, S., Eur. J. Biochem., **1995**. **227**: p. 823-828.

14.   Von Hippel, P.H., and Schleich, T., *Acc. Chem. Res.*, **1969**. **2**: p. 257-265.

15.   Von Hippel, P.H., and Schleich, T., In Biological Macromolecules; Timasheff, SN., Fasman, GD. Marcel Dekker, New York, **1969**. **2**: p. 417-574.

16.   Collins, K.D., and Washabaugh, M.L., *Q. Rev. Biophys.*, **1985**. **18**: p. 323-432.

17.   Timasheff, S.N., *Curr. Opinion struct. Biol.*, **1992**. **2**: p. 35-39.

18.   Schiffer, C.A., and Dotsch, V., *Curr. Opin. In Biotech.*, **1996**. **7**: p. 428-432.

19.   Hofmeister, F., *Arch. Exp. Pathol. Pharmakol.*, **1888**. **24**: p. 247-260.

20.   Baldwin, R.L., *Biophysical J.*, **1996**. **71**: p. 2056-2063.

21.   Robinson, D.R., and Jencks, W.P., *J. Am. Chem. Soc.*, **1965**. **87**: p. 2470-2479.

22.   Jencks, W., in Catalysis in Chemistry and Enzymology, Dover, Mineola, NY,, **1987**: p. 358-392.

23.   Arakawa, T., and Timasheff, S. N., In Protein Structure and Function: A Practical Approach. Creighton, TE, IRL press, Oxford, **1996**: p. 349-364.

24.   Shortle, D., *FASEB journal.*, **1996**. **10**: p. 27-34.

25.   Smith, P.E., Marlow, G.E., and Pettitt, B.M., *J. Am. Chem. Soc.*, **1993**. **115**: p. 7493-7498.

26.   Timasheff, S.N., *Acc. Chem. Res.*, **1970**. **3**: p. 62-68.

27.   Arakawa, T., and Timasheff. S.N., *Biochemistry*, **1984**. **23**: p. 5912-5923.

28.   Arakawa, T., and Timasheff, S.N., *Biochemistry*, **1982**. **21**: p. 6545-6552.

29.   Arakawa, T., and Timasheff, S.N., *Biochemistry*, **1982**. **21**: p. 6536-6544.

30.   Arakawa, T., Bhat, R., and Timasheff, S.N., *Biochemistry*, **1990**. **29**: p. 1924-1931.

31.   Timasheff, S.N., *Biochemistry*, **1992**. **31**(41): p. 9857-9864.

32.   Kita, Y., Arakawa, T., Lin, T.Y., and Timasheff, S.N., *Biochemistry*, **1994**. **33**: p. 15178-15189.

33.   Jackson, M., Haris, P.I., and Chapman, D., *Biochimica et Biophysica Acta*, **1989**. **998**: p. 75-79.

34.   Kandori, H., *J. Am. Chem. Soc.*, **1998**. **120**: p. 4546-4547.

35.   Venyaminov, S.Y., and Kalnin, N.N., *Biopolymers*, **1990**. **30**: p. 1243-1247.

36.   Susi, H., Timasheff, S.N., and Stevens, L., *J. Biol. Chem.*, **1967**. **242**: p. 5460-5466.

37. Arunkumar, A.I., Kumar, T.K., Sivaraman, T., and Yu, C., *Int. J. Biol. Macromol.*, **1997. 21**: p. 299-305.

38. Fabian, H., and Mantsch, H.H., *Biochemistry*, **1995. 34**: p. 13651-13655.

39. Reinstadler, D., Fabian, H.H., Backmann, J., Naumann, D., *Biochemistry*, **1996. 35**: p. 15822-15830.

40. From, N.B., and Bowler, B.E., *Biochemistry*, **1998. 37**: p. 1623-1631.

41. Nishimura, S., Sasaki, J., Kandori, H., Matsuda, T., Fukuda, Y., and Maeda, A., *Biochemistry*, **1996. 35**: p. 13267-13271.

42. Slaich, P.P., WU.; Robinson, DH.; Wharton, CW.; White, AJ.; Drabble, K.; Roberts, GC., *Biochem. J.*, **1992. 288**: p. 167-173.

43. Hehre, W.J., Radom, L., Schleyer, P.V.R., and Pople, J.A., in *Ab Initio Molecular Orbital Theory*, John Wiley & Sons, New York, **1986**.

44. Becke, A.D., *J.Chem.Phys*, **1993. 98**: p. 5648.

45. M. J. Frisch, G.W.T., H. B. Schlegel, G. E. Scuseria, M. A. Robb, J. R. Cheeseman, V. G. Zakrzewski, J. A. Montgomery, Jr., R. E. Stratmann, J. C. Burant, S. Dapprich, J. M. Millam, A. D. Daniels, K. N. Kudin, M. C. Strain, O. Farkas, J. Tomasi, V. Barone, M. Cossi, R. Cammi, B. Mennucci, C. Pomelli, C. Adamo, S. Clifford, J. Ochterski, G. A. Petersson, P. Y. Ayala, Q. Cui, K. Morokuma, D. K. Malick, A. D. Rabuck, K. Raghavachari, J. B. Foresman, J. Cioslowski, J. V. Ortiz, A. G. Baboul, B. B. Stefanov, G. Liu, A. Liashenko, P. Piskorz, I. Komaromi, R. Gomperts, R. L. Martin, D. J. Fox, T. Keith, M. A. Al-Laham, C. Y. Peng, A. Nanayakkara, M. Challacombe, P. M. W. Gill, B. Johnson, W. Chen, M. W. Wong, J. L. Andres, C. Gonzalez, M. Head-Gordon, E. S. Replogle, and J. A. Pople, *Gaussian, Inc.*, Pittsburgh PA, **1998**.

46. Schlegel, H.B., *J. Comp. Chem*, **1982. 3**: p. 214-218.

47.   Ochterski, J.W., in *Thermochemistry in Gaussian*, Gaussian Inc., **2000**.

48.   Radom, L., and Scott, A.P., *J. Phys. Chem*, **1996. 100**: p. 16502-16513.

49.   Reed, A.E., Curtiss, L.A., Weinhold, F., *Chem. Rev.*, **1988. 88**: p. 899-926.

50.   Weinhold, F., *NBO 4.M Program Manual*, Theoretical chemistry Institute and Department of Chemistry, University of Wisconsin; Madison, Wisconsin, **1996-1999**.

51.   Scott, A.P., and Radom, L., *J. Phys. Chem.*, **1996.** *100*: p. 16502-16513.

52.   Kalra, A., Tugcu, N., Cramer, S.M., and Garde, S., *J. Phys. Chem. B*, **2001.** *105*: p. 6380-6386.

53.   Hribar, B., Southall, N.T., Vlachy, V., and Dill, K.A., J. Am. Chem. Soc, **2002. 124**: p. 12302-12311.

54.   Dunford, H.B., in *Peroxidases in Chemistry and Biology* (Everse, J., Everse, K. E., and Grisham, M. B., Eds.) CRC Press, Boca Raton, FL., **1991. Vol. II**: p. pp 1-24.

55.   Chattopadhyay, K., and Mazumdar, S., *Biochemistry*, **2000.** *39*: p. 263-270.

56.   Tijssen, P., and Kurstak, E., *Anal. Biochem.*, **1984.** *136*: p. 451.

57.   Maidan, R., and Heller, A., *J. Am. Chem. Soc.*, **1991.** *11*: p. 9003-9004.

58.   Garguilo, M.G., Huynh, N., Proctor, A., and Michael, C.A., *Anal. Chem.*, **1993.** *65*: p. 523-528.

59.   Mondal, M.S., Mazumdar, S., and Mitra, S., *Inorg.Chem.*, **1993.** *32*: p. 5362.

60.   Modi, S., Saxena, A. K., Behere, D. V., and Mitra, S., *Biochim. Biophys. Acta*, **1990.** *1038*: p. 164-171.

61.   Gajhede, M., Schuller, D.J., Henriksen, A., Smith, A.T., and Poulos, T.L., *Nat. Struct. Biol.*, **1997. 4**: p. 1032-1038.

62.   Thanabal, V., Ropp, J. S. D., and La Mar, G. N., *J. Am. Chem. Soc.*, **1988.** *110*: p. 3027-3035.

63.   Tsaprailis, G.T., Chan, D.W.S., and English, A.M., *Biochemistry*, **1998**. *37*: p. 2004-2016.

64.   Holzbaur, I.E., English, A.M., and Ismail, A.A., *Biochemistry*, **1996**. *35*: p. 5488-5494.

65.   Coletta, M., Ascoli, F., Brunori, M., and Traylor, T.G., *J.Biol. Chem*, **1986**. *261*: p. 9811.

66.   Miller, M.A., Mauro, M.J., Smulevich, G., Coletta, M., Kraut, J., and Traylor, T.G., *Biochemistry*, **1990**. *29*: p. 9978-9988.

67.   Showen, K.J.B., in *Transition states of Biochemical processes, Plenum Press*, **1978**.

68.   Pappa, H.S., and Cass, A.E.G., *Eur. J. Biochem.*, **1993**. *212*: p. 227.

69.   Surewicz, W.K., Mantsch, H.H., and Chapman, D., *Biochemistry*, **1993**. *32*: p. 289.

70.   van Stokkum, I.H.M., Linsdell, H., Hadden, J.M., Haris, P.I., Chapman, D., and Bloemendal, M., *Biochemistry*, **1995**. *34*: p. 10518.

71.   Krimm, S., and Bandekar, J., *AdV. Protein Chem*, **1986**. *38*: p. 181-386.

72.   Barlow, C.H., Ohlsson, P.-I., and Paul, K. G., *Biochemistry*, **1976**. *15*: p. 2225-2229.

73.   Holzbaur, I.S., English, A. M., and Ismail, A. A., *J. Am. Chem. Soc*, **1996**. *118*: p. 3354-3359.

74.   Smith, M.L., Ohlsson, P.-I., and Paul, K.G., *FEBS Lett*, **1983**. *163*: p. 303.

75.   Uno, T., Nishimura, Y., Tsuboi, M., Makino, R., Iizuka, T., and Ishimura, Y., *J. Biol. Chem.*, **1987**. *262*: p. 4549.

76.   Li, T., Quillin, M.L., Phillips, G.N., and Olson, J.S., *Biochemistry*, **1994**. *33*: p. 1433-1446.

77.   Sears, D.W., and Beychock, S., in *Physical Principles and Techniques of Protein Chemistry* (Leach, S. J., Ed.) Part C, Academic Press, New York/London., **1973**: p. 445-593.

78. Hochstrasser, R.M., and Negus, D. K., *Proc. Natl. Acad. Sci., U.S.*A., **1984**. *81*: p. 4399-4403.

79. Forster, T.H., *Ann. Phys*, **1948**. **2**: p. 55-75.

80. Forster, T.H., in *Modern Quantum Chemistry, Part III* (Sinanoglu, O., Ed.) Academic Press, New York., **1965**. **Vol. 3**: p. pp 93-137.

81. Cheung, H.C., in *Topics in Fluorescence Spectroscopy* (Lakowicz, J. R., Ed.) , Plenum, New York., **1991**. **Vol. 2, Chapter 3**.

82. Burnstein, E.A., Vedenkina, N. S., and Ivkova, M. N., *Photochem. Photobiol.*, **1973**. *18,*: p. 263-269.

APPENDICES

Appendix A
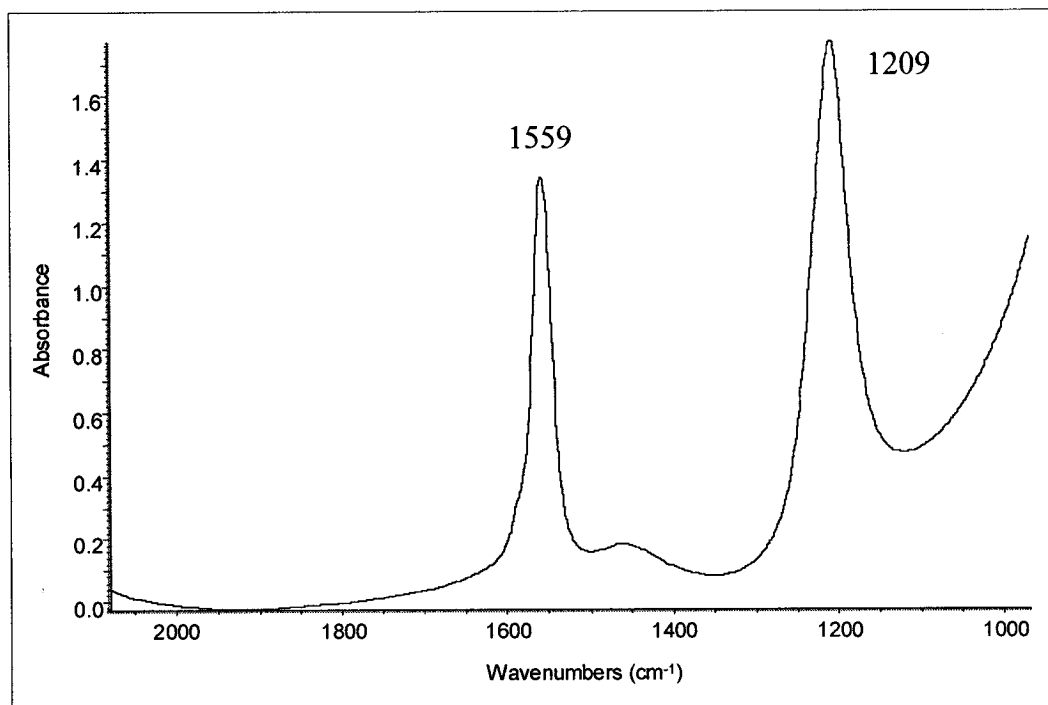
FTIR spectrum of 1 M ^{13}C-GdnDCl. The peaks at 1559 cm^{-1} and 1209 cm^{-1} are assigned to $\nu(^{13}CN)$ of ^{13}C-GdnDCl and $\delta(OD)$ of D_2O, respectively. The FTIR spectrum is an average of 500 scans acquired at a resolution of 2 cm^{-1} at pH 6.2 and 25°C. Solutions were prepared by weight by dissolving the salt in D_2O and 7 μL of solution was placed on a CaF$_2$ window. The FTIR cell was assembled using 6 μm spacers.
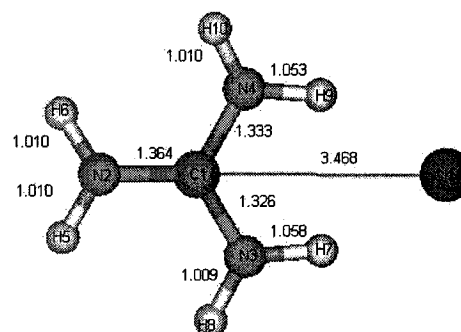
Appendix B
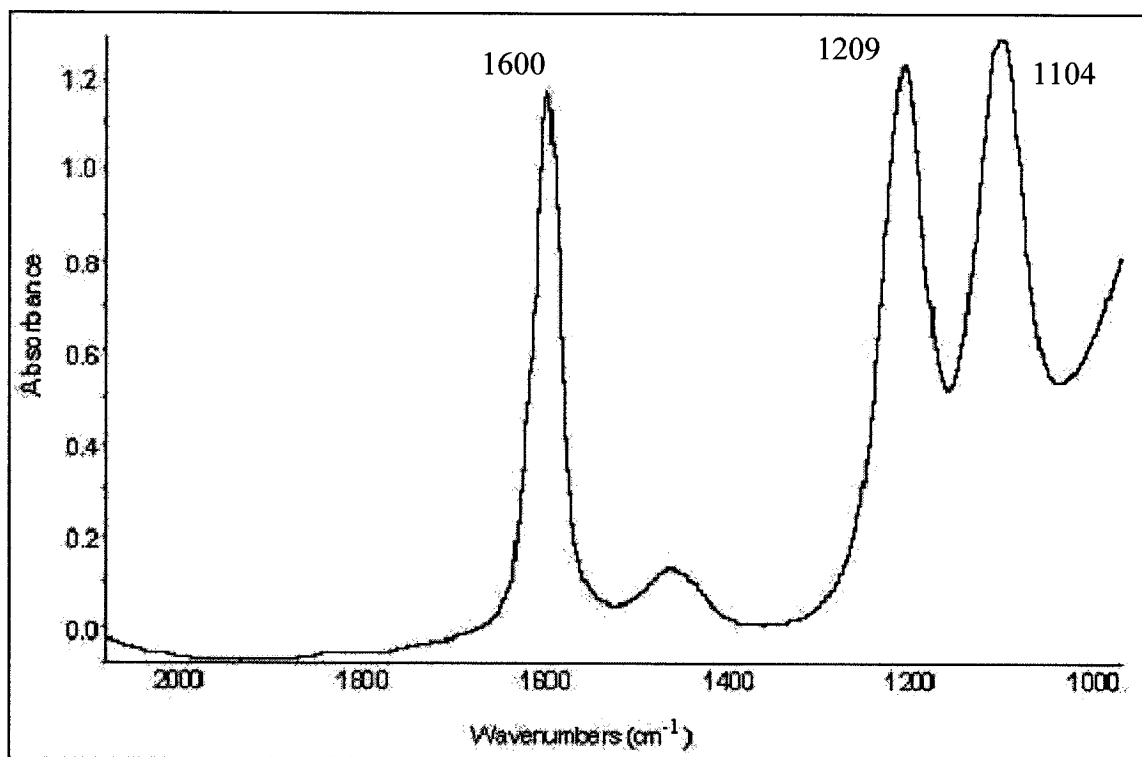
FTIR spectrum of 1 M $GdnD_2SO_4$. The peaks at 1600 cm^{-1}, 1209 cm^{-1} and 1104 cm^{-1} are assigned to $\nu(CN)$ of $GdnD_2SO_4$, $\delta(OD)$ of D_2O and $\nu(SO_4)$, respectively. The FTIR spectrum is an average of 500 scans acquired at a resolution of 2 cm^{-1} at pH 6.2 and 25°C. Solutions were prepared by weight by dissolving the salt in D_2O and 7 μL of solution was placed on a CaF_2 window. The FTIR cell was assembled using 6 μm spacers.
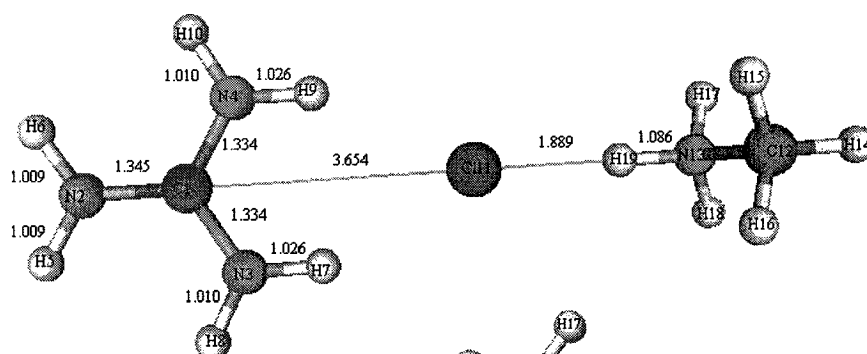
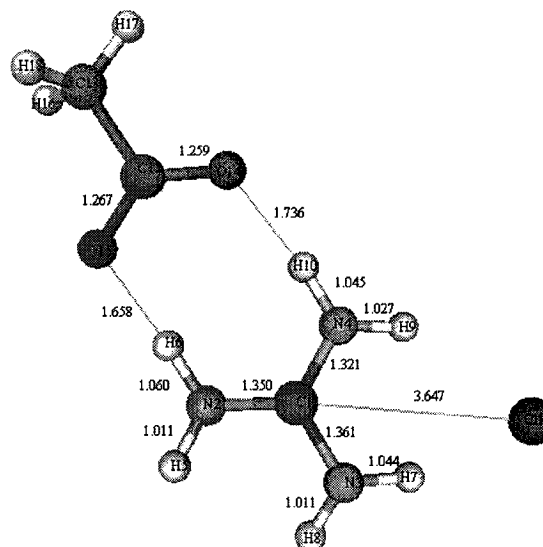**Appendix C**

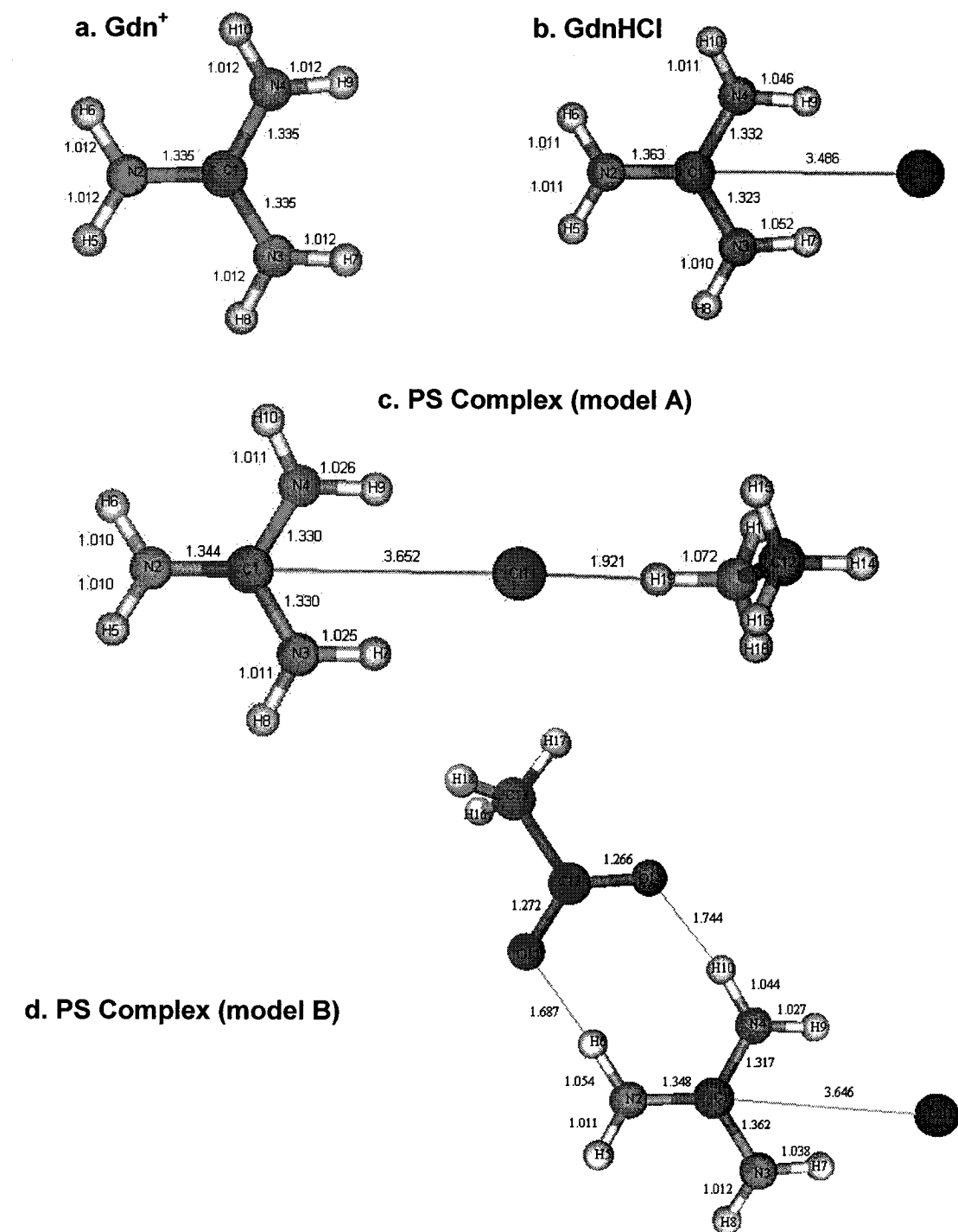## a. Gdn⁺
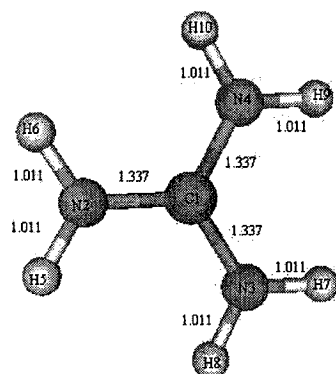
b. GdnHCl

c. PS Complex (model A)

d. PS Complex (model B)

Molecular geometries of Gdn⁺, GdnHCl and PS complex (model A and B) obtained with the B3LYP/6-31G* model chemistry. All distances are in Angstroms.

Appendix D

a. Gdn⁺

b. GdnHCl

c. PS Complex (model A)

d. PS Complex (model B)

Molecular geometries of Gdn⁺, GdnHCl and PS complex (model A and B) obtained with the MP2/6-31G* model chemistry. All distances are in Angstroms.